

UNCLASSIFIED

AD NUMBER: AD0805391

LIMITATION CHANGES

TO:

Approved for public release; distribution is unlimited.

FROM:

Distribution authorized to U.S. Gov't. agencies and their contractors; Administrative/Operational Use; 1 Dec 1966. Other requests shall be referred to Army Electronics Command, Fort Monmouth, NJ

AUTHORITY

AEC ltr 16 Jun 1971



UNCLASSIFIED

AD

805391

PHONON INTERACTIONS IN CRYSTALS

FINAL QUARTERLY TECHNICAL REPORT

DECEMBER 1966

.....
E COM

UNITED STATES ARMY ELECTRONICS COMMAND · FORT MONMOUTH, N.J.

CONTRACT DA 36-039 AMC-02280 (E)

INTERNATIONAL BUSINESS MACHINES CORP.

**Thomas J. Watson Research Center
Yorktown Heights, N. Y.**

This document is subject to special export controls and each transmittal to foreign governments or foreign nationals may be made only with prior approval of Commanding General, U. S. Army Electronics Command, Fort Monmouth, New Jersey, AMSEL-KL-SM.

2

PHONON INTERACTIONS IN CRYSTALS

Contract DA 36-039-AMC-02280(E)

FINAL REPORT

Prepared by

M. Pomerantz, P. B. Miller, N. S. Shiren, and R. J. von Gutfield

INTERNATIONAL BUSINESS MACHINES CORPORATION

T. J. Watson Research Center

P. O. Box 218

Yorktown Heights, New York 10598

This document is subject to special export controls and each transmittal to foreign governments or foreign nationals may be made only with prior approval of Commanding General, U. S. Army Electronics Command, Fort Monmouth, New Jersey, AMSEL-KL-SM.

Work Performed for U. S. Army Electronics Command
Fort Monmouth, New Jersey 07703

BLANK PAGE

TABLE OF CONTENTS

Purpose

Abstract

Publications

Factual Data

Work Completed Since the 12th Quarterly Report:

Part I Spin Lattice Relaxation and Generation of Phonon Avalanches in $S = 1$ Systems

Part II The Temperature Dependence of Heat Pulse Propagation in Sapphire

Part III Detection of Ultrasound Using Thin Film Bolometers

Summary of Work Under Contract DA36-039AMC-02280(E):

Part I Phonon-Phonon Interaction

Part II Phonon Interaction with Paramagnetic Ions

Part III Phonon Interaction with Static Defects

Part IV Phonon Interactions with Free Electrons

Conclusions

PURPOSE

The purpose of this contract is to investigate, experimentally and theoretically, various interaction processes of phonons in solids with a view towards developing and improving methods of amplifying, generating, frequency converting, and propagating microwave acoustic energy.

One main approach is to study the parametric amplification and parametric frequency conversion of acoustic waves, especially the forward traveling wave interaction. These interactions are being studied in various materials. The use of paramagnetic ions in magnesium oxide has been investigated to maximize such effects.

Another approach is to study the transfer of energy to the acoustic waves from electrons whose drift velocity is greater than the velocity of sound. This amplification process has previously been observed for piezoelectric materials, but had not been demonstrated for materials like germanium where the deformation potential is responsible for the electron - phonon interaction. A substantial acoustic gain at microwave frequencies has now been achieved in Ge.

Microwave acoustic masers are also being studied as amplifiers. For reasons of basic scientific interest, signal velocity effects are being measured in such acoustic maser amplifiers.

Various sound propagation effects are also under investigation, especially the attenuation of microwave phonons in germanium and other materials as a function of temperature.

3.

Heat pulses are being used to study energy propagation effects,
attenuation, and scattering of quasi-thermal phonons in solids.

ABSTRACT

Spin lattice relaxation to a phonon bottlenecked lattice has been observed in Fe^{2+} and Ni^{2+} doped MgO . The Ni^{2+} spin system was studied extensively. Avalanche relaxation was observed for both the $\Delta M = 2$ and $\Delta M = 1$ transitions at 2°K with characteristic avalanche times of $\sim 4 \times 10^{-7}$ sec and 2×10^{-6} sec respectively in material having a doping concentration of $8 \times 10^{18}/\text{cm}^3$. The expected line shape "inversion" has also been observed. For Fe^{2+} with a concentration of $2 \times 10^{18}/\text{cm}^3$ the calculated avalanche time constant is 4×10^{-8} sec. This time is short enough to allow avalanche formation in a small volume of crystal and phonons generated by an avalanche at one end of a 2.5 cm long rod were detected at the other end. It was found that only a few phonons modes were excited, most of the modes remaining cold. The decay of the hot phonons then occurs primarily through spin scattering to the cold modes at the spin resonance frequency.

Results of heat pulse measurements between $4^\circ \rightarrow 54^\circ\text{K}$ are reported for sapphire and show that the propagation is ballistic below 18°K and diffusive above 40°K . In the intermediate range, the propagation is a superposition of the two. No second sound is observed throughout this temperature range.

Microwave phonon echoes have been observed in AC and x-cut quartz crystals at 9.2 GHz using thin film detectors. These detectors are similar to those used in heat pulse experiments and are capable of detecting incoherent phonons. Echoes have been observed with In-Sn films in the intermediate state (1.4-3.8°K) as well as pure In films in the normal state, up to ~ 12°K. Throughout this temperature range, modulation effects in the echo pattern, similar to those observed in superconducting tunneling experiments, were also observed. The attenuation of the echo pattern appears to be considerably larger than expected from existing attenuation data and the Pippard theory of phonon attenuation in metals.

The remainder of this Final Report is a summary of all the work pursued under the contract.

Papers Published since 12th Quarterly Report.

R. J. von Gutfeld, "Temperature Dependence of Heat Pulse

Propagation in Sapphire", Phys. Rev. Lett. 17, 868 (1966).

R. J. von Gutfeld, "Thermal Relaxation of Indium Films on

Insulating Substrates between 4°K and 300°K ", J. Appl. Phys.

37, 3767 (1966).

P. B. Miller, "Attenuation of High Energy Transverse Phonons",

Phys. Rev. 146, 592 (1966).

N. S. Shiren, "Observation of Phonons Generated in Paramagnetic

Relaxation", Phys. Rev. Lett. 17, 958 (1966).

7.

I. Spin Lattice Relaxation and Generation of Phonon Avalanches in $S=1$ Systems

I Introduction

The effect of a phonon bottleneck on spin lattice relaxation was first considered by Van Vleck in 1941.¹ Since then considerable theoretical and experimental investigations have been undertaken.² Until 1965 all of the experimental evidence for the presence of a bottleneck was based on observations of size and concentration dependent relaxation times, either in cw experiments or in measurements of the decay of the magnetization following a saturating microwave signal. More recently an observation of spin lattice relaxation by phonon avalanche from an inverted population has been reported in $(La, Ce)_2 Mg_3 (NO_3)_{12} \cdot 24H_2O$ by Brya and Wagner.^{3, 4} Similar observations have been made by us in $Ni^{2+} : MgO$, and indirect evidence for avalanche relaxation was obtained in very dilute concentrations of Fe^{2+} in MgO .^{5, 6}

Our experiments were performed at $\sim 2^{\circ}K$ and were similar to those of Brya and Wagner. Adiabatic rapid passage was used to invert the spin populations and the transitions were then observed, as a function of time after the passage was completed, by means of a low amplitude probing signal. In our experiments both electromagnetic and ultrasonic probes were used. The ultrasonic probe has the advantage of not requiring doubly resonant cavity structures and thereby allowing a wide range of probing frequencies. (Measurements were made at both X and

8.

Ku bands.) Details of the experimental apparatus and technique have been reported previously.⁶

The $S = 1$ ions, Ni^{2+} and Fe^{2+} , have the disadvantage, compared with the $S = 1/2$ ion, Ce, that because relaxation occurs in both $\Delta M = 1$ and $\Delta M = 2$ transitions, there is an added complexity in analyzing the results. However, in MgO , because of the random distribution of local crystal fields, there is a distribution of zero field splittings and this allows the use of sequential inversion of the spin packets making up the inhomogeneously broadened $\Delta M = 1$ resonances. This results in some parts of the line being inverted with \sim twice their equilibrium population differences. By stopping the passage before completely traversing the line it was also possible to invert some of the $\Delta M = 1$ transitions while maintaining the $\Delta M = 2$ transition uninverted. The use of $S = 1$ ions also allowed observation of the phonon-photon $\Delta M = 2$ transition which, in the Fe^{2+} system, was the only observable inverted transition.

In samples with Ni^{2+} concentrations of about $10^{18}/\text{cm}^3$ our results were very similar to those of Brya and Wagner on Ce with about the same concentration. This is to be expected since in the presence of a strong bottleneck the only important parameters governing the avalanche formation at a given temperature are

the concentration and the intrinsic direct process relaxation time, T_1 . At 2°K, T_1 for both ions is of order 10^{-2} sec.

In the case of Fe^{2+} however, only indirect evidence for avalanche relaxation was obtained. Following rapid passage no net inversion was observed, the transitions were saturated, except under the condition necessary for observation of photon-phonon double quantum emission;^{5, 6} i. e., the RF pulse used in the passage was left on after completion of the sweep for a time long enough for the probing ultrasonic signal to traverse the crystal. Even under this condition, however, the observed ultrasonic gain was smaller than expected from a fully inverted system by up to two orders of magnitude. It was also observed that the gain was independent of concentration over the range $10^{16} - 10^{18}/\text{cm}^3$. While the effect of the strong RF field on the relaxation behavior is not yet understood, it will be shown below that these observations are consistent with the presence of avalanche relaxation of a spin system with $T_1 \sim 10^{-4}$ sec appropriate to Fe^{2+} in MgO. Furthermore while as stated above, the avalanche of the spin system could not be observed, we have recently succeeded in detecting the phonons generated by this avalanche. These observations will be discussed in Sec. IV.

II Theory of Avalanche Relaxation

The rate equations for a two level spin system interacting

with the lattice phonons are,

$$\frac{dp(\omega)}{dt} = - \int d\omega' \sum_{\kappa\lambda} W_{\kappa\lambda}(\omega') \rho_{\kappa\lambda}(\omega') [n(\omega') [2p_{\kappa\lambda}(\omega') + 1] - n_0(\omega) [2p_{\kappa\lambda}(\omega') + 1]] \quad (1)$$

$$\sum_{\kappa\lambda} \rho_{\kappa\lambda}(\omega') \frac{dp_{\kappa\lambda}(\omega)}{dt} = \frac{1}{2} \frac{dp(\omega)}{dt} - \frac{1}{T_p} \sum_{\kappa\lambda} \rho_{\kappa\lambda}(\omega) [p_{\kappa\lambda}(\omega) - p_{0\kappa\lambda}(\omega)] \quad (2)$$

where: $n(\omega) = (N_1 - N_2)h(\omega)$ is the population difference per unit frequency per cm^3 in an inhomogeneously broadened line with normalized line shape $h(\omega)$; N_1 and N_2 are the populations of the lower and upper levels respectively; $p_{\kappa\lambda}(\omega)$ is the mean occupation number of the phonon mode with propagation vector $\vec{\kappa}$ and polarization $\vec{\lambda}$; $\rho_{\kappa\lambda}(\omega)$ is the density of modes per unit frequency of type $\vec{\kappa}\vec{\lambda}$ at ω . The subscript, o, refers to equilibrium values, and T_p is the time constant for decay of the phonons to the bath, which includes all phonons not interacting with the spin system. $W_{\kappa\lambda}$ is the transition rate per phonon/ cm^3 .

$$W_{\kappa\lambda}(\omega') = \frac{\pi\omega' G_{\kappa\lambda}^2}{\hbar\rho v_{\kappa\lambda}} g(\omega' - \omega)$$

where $g(\omega' - \omega)$ is the normalized homogeneous line shape peaked at ω . $G_{\kappa\lambda}$ is a spin phonon coupling constant which, in

general, is a function of the angle between the magnetic field, \vec{H} , and $\vec{\kappa}$, $\vec{\lambda}$. $v_{\kappa\lambda}$ is the velocity of the $\vec{\kappa}$, $\vec{\lambda}$ mode and ρ is the crystal density. Under the assumption that $g(\omega)$ is much sharper than any of the other frequency functions we have,

$$\int d\omega' W_{\kappa\lambda}(\omega') \rho_{\kappa\lambda}(\omega') n(\omega') p_{\kappa\lambda}(\omega') = \frac{\pi\omega G_{\kappa\lambda}^2}{\hbar \rho v_{\kappa\lambda}^2} \rho_{\kappa\lambda}(\omega) n(\omega) p_{\kappa\lambda}(\omega)$$

and

$$\sum_{\kappa\lambda} \frac{\pi\omega G_{\kappa\lambda}^2}{\hbar \rho v_{\kappa\lambda}^2} \rho_{\kappa\lambda}(\omega) [2p_{0\kappa\lambda}(\omega) + 1] = \frac{1}{T_1}$$

T_1 is the intrinsic relaxation rate in the absence of bottleneck effects.

We now write for the total number of phonons per unit frequency at ω ,

$$p(\omega) = \sum_{\kappa\lambda} \rho_{\kappa\lambda}(\omega) p_{\kappa\lambda}(\omega)$$

and let
$$b(\omega) = \sum_{\kappa\lambda} \rho_{\kappa\lambda}(\omega).$$

We also make the approximation

$$A = \frac{\pi\omega \langle G^2 \rangle}{\hbar \rho \langle v^2 \rangle} = \frac{\sum_{\kappa\lambda} \frac{\pi\omega G_{\kappa\lambda}^2}{\hbar \rho v_{\kappa\lambda}^2} \rho_{\kappa\lambda}(\omega)}{\sum_{\kappa\lambda} \rho_{\kappa\lambda}(\omega)} = \frac{1}{(2p_0 + b) T_1}$$

since $p_{0\kappa\lambda}(\omega)$ is independent of $\vec{\kappa}$, $\vec{\lambda}$.

12.

Then Eq's. (1) and (2) become,

$$\frac{dn}{dt} = -A [n(2p+b) - n_o(2p_o+b)], \quad (1')$$

$$\frac{dp}{dt} = \frac{1}{2} \frac{dn}{dt} - \frac{p-p_o}{T_p}, \quad (2')$$

where we have omitted the arguments, (ω). The equations may be solved analytically under the condition, $\frac{1}{2} \left| \frac{dn}{dt} \right| \gg \frac{p-p_o}{T_p}$, which will be seen to apply in most of the cases of interest here.

The solutions are

$$\frac{1}{2}(n - n_i) = (p - p_o) = -\frac{1}{2} \frac{(a+\beta)(1 - \exp \beta A t)}{1 - \frac{a+\beta}{a-\beta} \exp \beta A t} \quad (3)$$

$n_i(\omega)$ is the initial population difference at $t = 0$ following rapid passage and

$$a = (2p_o + b) + n_i,$$

$$\beta = [n_i^2 - 2n_i(2p_o + b) + 4n_o(2p_o + b) + (2p_o + b)^2]^{1/2}.$$

When the inversion level is sufficiently strong and the temperature low enough so that $|n_i| \gg p_o, b$ we have,

$$a - \beta \approx (2p_o + b) \left(1 - \frac{2n_o - n_i}{n_i} \right),$$

$$a + \beta = 2n_i,$$

$$\beta \approx n_i \left[1 + \frac{(2n_o - n_i)(2p_o + b)}{n_i^2} \right] = n_i.$$

Writing $n_i = -\sigma n_o$, where σ is the inversion ratio,

$$n = -\sigma n_o \frac{(1+B)t^{-t/\tau}}{1+Bt^{-t/\tau}} \quad (4)$$

$$p = p_o + \sigma n_o \frac{1-t^{-t/\tau}}{1+Bt^{-t/\tau}} \quad (5)$$

where: $\tau = -(\beta A)^{-1} = ((2p_o + b)/\sigma n_o) T_1 \ll T_1$. (6)

and $B = \sigma^2 n_o / (1 + \sigma)(2p_o + b) = (\sigma / 1 + \sigma)(T_1 / \tau)$. (7)

τ is equivalent to the constant T'_b defined by Scott and Jeffries.⁷

In Fig. 1 we have graphed Eq.(4) for $\sigma = 1$. Experimental curves of this type, which clearly show the pedestal, during which the population remains almost constant, followed by the relaxation avalanche, have been published by Brya and Wagner.³ As a measure of the length of the pedestal we may take the time t' at which the derivative of n or p reaches its maximum,

$$t' = \tau \log_e B. \quad (8)$$

Since B may be very large, of order $10^4 - 10^5$, the dominant variation of t' with σ is as σ^{-1} . This behavior also appears in the data of Ref. 3.

III Experimental Measurements on the Spin Systems

In treating the $S = 1$ systems the rate equations (1) and (2) are, of course, incorrect. However, as pointed out earlier,

by use of incomplete sequential passage (see Quarterly Report No. 6) it was possible to invert some of the $\Delta M = 1$ transitions while leaving the complementary ones, and the $\Delta M = 2$ transitions, normal. Under this condition, the inverted transitions will avalanche in times short compared with the normal T_1 decay of the others and the inverted transitions may then be treated as an isolated $S' = 1/2$ system.

Under other conditions of passage some of the $\Delta M = 1$ transitions are inverted to twice their equilibrium populations, while the complementary ones remain normal and the $\Delta M = 2$ transition is inverted to half its equilibrium population. Because of frequency factors the $\Delta M = 2$ transition then avalanches much faster than $\Delta M = 1$. The two transitions behave as almost isolated $S' = 1/2$ systems. The former starts with an initial population, $-n_0$, and avalanches to saturation, leaving the latter with an effective initial population, $-3/2 n_0$. (n_0 is here the equilibrium $\Delta M = 1$ value.) An experimental curve exhibiting this behavior is shown in Fig. 2. The data were taken on an MgO sample containing approximately $8 \times 10^{18}/\text{cm}^3$ Ni^{2+} ions, and having a line width of ~ 100 oe. At 2°K , $n_0(\omega) = 6 \times 10^8/\text{cm}^3/\text{Hz}$. Under the assumption that all transverse modes have the velocity of the transverse mode propagating on the $\langle 100 \rangle$ axis,

15.

$v_t = 6.68 \times 10^5$ cm/sec, and the analogous assumption for longitudinal modes, $v_l = 9.25 \times 10^5$ cm/sec, we find at $\omega/2\pi = 9.0$ GHz and 2°K ,

$$\sum_{\kappa\lambda} \rho_{\kappa\lambda} (2p_{\text{OK}\lambda} + 1) = (2p_o + b)_1 = 1.3 \times 10^4 / \text{cm}^3 / \text{Hz},$$

while for the modes interacting with $\Delta M = 2$ at 18 GHz,

$$(2p_o + b)_2 = 2.6 \times 10^4 / \text{cm}^3 / \text{Hz}.$$

The calculated relaxation times are 0.13/sec and .01/sec for $\Delta M = 1$ and $\Delta M = 2$ respectively. Thus, using the initial conditions given above we find

$$\tau_1 = 1.9 \times 10^{-6} \text{ sec}, \quad B_1 = 2.9 \times 10^4$$

$$\tau_2 = 4.3 \times 10^{-7} \text{ sec}, \quad B_2 = 1.1 \times 10^4$$

and

$$t'_1 = 2 \times 10^{-5} \text{ sec}$$

$$t'_2 = 4 \times 10^{-6} \text{ sec}$$

The measured values from Fig. 2 are about a factor 2 larger, which probably reflects the inaccuracy in the computed values of T_1 .

When, as noted above, various parts of the inhomogeneously broadened line have different levels of inversion, we may consider

σ to be a function of the magnetic field at which observations are made at the probing frequency, i. e. $\sigma = \sigma(H)$. Then both T and B (and therefore t') will exhibit this dependence. Since t' is roughly inversely proportional to $\sigma(H)$ the line shape will appear to invert during the relaxation process. This is demonstrated in Fig. 3 which shows a Ni^{2+} line shape observed at several times following passage, using an ultrasonic probing signal and sampling techniques. (The value of $n_0(\omega)$ was somewhat larger for this sample than for that of Fig. 2.) The line was only partially swept during the passage and many passages were made while the D. C. field was slowly varied. Thus each point on the abscissa represents a different experiment. Because an ultrasonic probe was used the ordinates are proportional to $\exp[\gamma \sigma(H) n(t)]$, where γ is a constant. At time $t = 0$, in Fig. 3, the $\Delta M = 2$ avalanche has already occurred for those parts of the line for which it is applicable. The large peak thus represents an inversion level $\sigma = 3/2$, while the smaller peak corresponds to $\sigma = 1$. The variation of t' with $[\sigma(H)]^{-1}$, leading to an apparent self-reversal is clear.

We now turn our attention to the relaxation of Fe^{2+} . As noted previously, following rapid passage no inversion was measured in any of our samples except under the conditions

necessary for phonon-photon double quantum amplification, and then the observed gain was almost constant among crystals containing varying concentrations of Fe^{2+} .

The highest concentration sample contained $2 \times 10^{18}/\text{cm}^3$ Fe^{2+} ions, and for the $\Delta M = 1$ transitions we find, with $G = 1$,

$$\tau = 4 \times 10^{-8}, \quad B = 1.2 \times 10^3$$

giving,

$$t' = 2.8 \times 10^{-7} \text{ sec.}$$

In our most dilute sample the concentration was $\sim 5 \times 10^{16}/\text{cm}^3$. The calculated t' is thus $\sim 10^{-5}$ sec.

Our measurements of the ultrasonic gain in Fe^{2+} double quantum transitions indicate that the effective values of t' must be a factor ~ 10 smaller than calculated above. Such fast avalanche relaxation also explains the observation, mentioned earlier, that the observed gain was almost independent of concentrations. If t' is shorter than the propagation time of the ultrasonic pulse through the crystal ($\sim 1\text{-}2\mu\text{sec}$) then the gain constant (which is proportional to $n(t)$) is proportional to the product, $n_0 t'$, which is only logarithmically dependent on n_0 .

A possible explanation for the discrepancy between theory and experiment is as follows. Brya and Wagner have pointed out that an avalanche is inhibited during the sweep because the

resonance line is not allowed to dwell at any one frequency long enough. However, this effect will only take place for inhomogeneously broadened lines if the line width is narrow compared with the extent of the sweep and the time during which the line is swept is small compared with t' . This is the case for the Ni^{2+} which is about 35-100 gauss wide (varying among different crystals) and has $t' \sim 10^{-5}$ as compared with the sweep which goes through ~ 1000 gauss in $2.5 \mu\text{sec}$. However, in the case of Fe^{2+} , the line is of order 400 gauss wide (peak-peak derivative). There are always phonons generated initially from spin packets which are inverted at the start of the sweep. These phonons come into resonance with spin packets which are inverted later on; therefore these spins see higher than equilibrium phonon populations. The spin systems will thus avalanche faster than predicted by the above calculations and the relaxation process will begin earlier. (Actually our solutions, Eq's. (4) and (5) may no longer be valid because of the assumption that $|n_1| \gg p_1$.)

IV Observation of the Phonons

In this section we discuss the detection of phonons generated in paramagnetic spin lattice relaxation. The phonons were generated at one end of an Fe^{2+} doped MgO rod (0.3 cm diameter, 2.5 cm long) following adiabatic rapid passage

inversion and the consequent avalanche relaxation to a bottlenecked lattice. They were observed at the other end of the rod by the phonon-photon double quantum detection technique.⁸ Several unsuccessful attempts utilizing a similar geometry, but saturating rather than inverting the spins at the generator end of the rod, have been reported in the literature.^{9, 10, 11} The phonon flux density in the avalanche is several orders of magnitude greater than can be obtained by saturation, and in the present experiments, also, no phonons were detected when only a saturating microwave pulse was applied; it was always necessary to have both the microwave pulse and the field sweep simultaneously present, thereby producing population inversion.

Measurements were made on several crystals, 0.3 cm diameter by 2.5-3 cm long, oriented with the rod axis parallel to the $\langle 100 \rangle$ crystallographic direction, and containing Fe^{2+} concentrations of about 100 ppm. In some experiments two short rods were bonded together with GE7031 resin so as to obtain the required overall length. The experiments were conducted at 1.9°K with the crystals immersed in the liquid He bath. Similar results were obtained on all runs. As a check to

be sure that the observed effect was not due to spin saturation at the detector by electromagnetic leakage, one run was made using a doped crystal and an undoped crystal bonded together, with the latter in the generator cavity. No detector pulse was obtained.

The length of crystal over which the spins were inverted is determined by the microwave field configuration and is thus not sharply defined. However, it was estimated to be about 1 cm, and the distance from the end of the inversion region to the detector cavity was also about 1 cm. The double quantum detection method has the disadvantage that its output at a given time is proportional to the phonon density integrated over the portion of the crystal (≥ 0.5 cm) within the detector cavity. Its effective response time was therefore too slow to provide detailed information on the risetime of the phonon pulse. However, the method was chosen over other possibilities, such as thin film bolometers¹² or Josephson junctions,¹³ because of its frequency selectivity and its sensitivity to phonon polarization. The latter could be adjusted by changing the direction of the external magnetic field with respect to the propagation direction.

The inhomogeneously broadened Fe^{2+} resonance is about 400 oe wide and therefore, following rapid passage there is a broad spectrum of inverted spin packets. However, by partially

passaging the line, sweeping down from high field and terminating at the D. C. field, H_0 , only spin packets at frequencies lower than or equal to that of the microwave pulse were inverted. Then since the Fe^{2+} double quantum line shape falls off sharply on the low frequency side, it was possible to set an upper limit of about 10 MHz on the width of the phonon modes. Unfortunately, the accuracy of this result is not sufficiently great to provide a check on the theoretical prediction² that the mode width should not be larger than the homogeneous spin packet width, estimated to be 2 MHz in our crystals.

A typical detected phonon pulse is shown in Fig. 4. The pump frequency was 8.790 GHz and the detector CW microwave frequency, 9.085 GHz. The detailed shape of the rise is washed out by the detection integration time. However, a delayed onset time, following inversion, and a linear rise over the first 2 or 3 microseconds indicate that the initial part of the pulse arrives by rectilinear propagation. Most of the energy, however, arrives by diffusion and a rough comparison with the solution of the diffusion equation for our geometry indicates a mean free path of about 1/2 cm, in approximate agreement with the value, 0.3 cm, expected on the basis of boundary scattering on the cylindrical surface.¹⁴

In Fig. 5 we have plotted measured pulse amplitudes as a

function of the angle θ between H_0 and the rod axis $\langle 100 \rangle$. Also shown are theoretical detection sensitivity curves for longitudinal waves, and transverse waves polarized in and perpendicular to the plane of rotation of H_0 , all propagating on $\langle 100 \rangle$. It is clear that in all of the experiments transverse waves predominated. The differences among various runs may be due to such factors as the presence of bonds in some cases. The angular distribution was also observed to fall off more sharply from the $\theta = 0^\circ$ value when the pump pulse was left on after termination of the sweep. This result is not unexpected since the spin-phonon transition probabilities are altered in the presence of a strong RF field and will, therefore, depend on the angular variations of the effective perpendicular component of that field. The preponderance of transverse waves is expected since a factor v^{-5} (where v is the phonon velocity) appears in the expression for the spin relaxation transition probability which is thus larger for transverse than longitudinal modes. As is the case in laser oscillators, small differences in the gain constant among different modes can lead to complete dominance of a few modes in the avalanche. The relative amplitudes of the modes constituting the phonon pulse is thus not the same as the relative relaxation rates and, contrary to the usual theoretical formulations

of the phonon bottleneck problem (e. g. Sec. II) most of the modes will not be heated.

The decay of the pulses in Fig. 4 is interpreted as follows. Because the length of the absorbing region is equal to or greater than the emission length, the generated phonons will be almost completely absorbed after a few passes through the crystal, resulting in partial saturation of the spin transitions at the phonon frequency. This produces an increased absorption signal (in addition to the true double quantum signal) at the detector frequency.⁸ The absorbed energy is then transferred to the cold phonon modes via spin lattice relaxation with a time constant approximately equal to the equilibrium temperature relaxation rate. This results in the observed nearly exponential decay of the detector output signal. The measured time constant is 420 microseconds, in close agreement with the spin lattice relaxation time measurements of Castle and Feldman.¹⁵ It may be noted that even if the excess generated phonon population were larger than the number of absorbing spins, the principal heat loss mechanism from the hot modes (after saturation of the spins) would still be transfer to the cold modes via spin scattering at the spin relaxation rate. This is considerably shorter than the rate for transfer via phonon-phonon scattering

as estimated from microwave ultrasonic attenuation measurements.¹⁶

The original reason for undertaking this investigation was the observation, previously reported, that inversion of Fe^{2+} spins after rapid passage was not directly observable ; and that this result was probably due to an extremely fast avalanche relaxation to saturation,⁶ with a time constant, 4×10^{-8} sec and a delay time (pedestal length) 3×10^{-7} sec.¹⁵ The present observations support this conclusion. Indeed, if the avalanche could not occur in a time short compared with the propagation time through the emission volume into the absorbing region, there would be no avalanche formation at all.

REFERENCES

1. J. H. Van Vleck, *Phys. Rev.* 59, 724 (1941).
2. J. A. Giordmaine and F. R. Nash, *Phys. Rev.* 138, 1510 (1965). This paper contains an extensive bibliography to the earlier literature.
3. W. J. Brya and P. E. Wagner, *Phys. Rev. Letters* 14, 431 (1965).
4. P. E. Wagner and W. J. Brya, *Physics of Quantum Electronics*, Ed. Kelley, Lax and Tannenwald, (McGraw-Hill Book Co., Inc., New York, 1966) p. 376.
5. N. S. Shiren, *Appl. Phys. Letters* 7, 142 (1965).
6. N. S. Shiren, *Physics of Quantum Electronics*, Ed. Kelley, Lax and Tannenwald, (McGraw-Hill Book Co., Inc., New York, 1966) p. 385. Also see Quarterly Report No. 7.
7. P. L. Scott and C. D. Jeffries, *Phys. Rev.* 127, 32 (1962).
8. N. S. Shiren, *Phys. Rev. Letters* 6, 168 (1961).
9. K. Dransfeld, *Bull. Am. Phys. Soc.* 3, 324 (1958).
10. N. S. Shiren and E. B. Tucker, *Phys. Rev. Letters* 2, 206 (1959).
11. B. W. Faughnan and M. W. P. Strandberg, *J. Phys. Chem. Solids* 19, 155 (1961).

26.

12. R. J. von Gutfeld, 1966 Ultrasonics Symposium, to be published.
13. B. Abeles and Y. Goldstein, *Phys. Rev. Letters* 14, 595 (1965).
14. H. B. G. Casimir, *Physica* 5, 495 (1938).
15. J. G. Castle and D. W. Feldman, quoted in: N. S. Shiren, Proceedings of the XI Colloque Ampere, Ed. J. Smidt (North Holland Publishing Co., Amsterdam, 1963) p. 114.
16. I. S. Ciccarello and K. Dransfeld, *Phys. Rev.* 134, A1517 (1964).

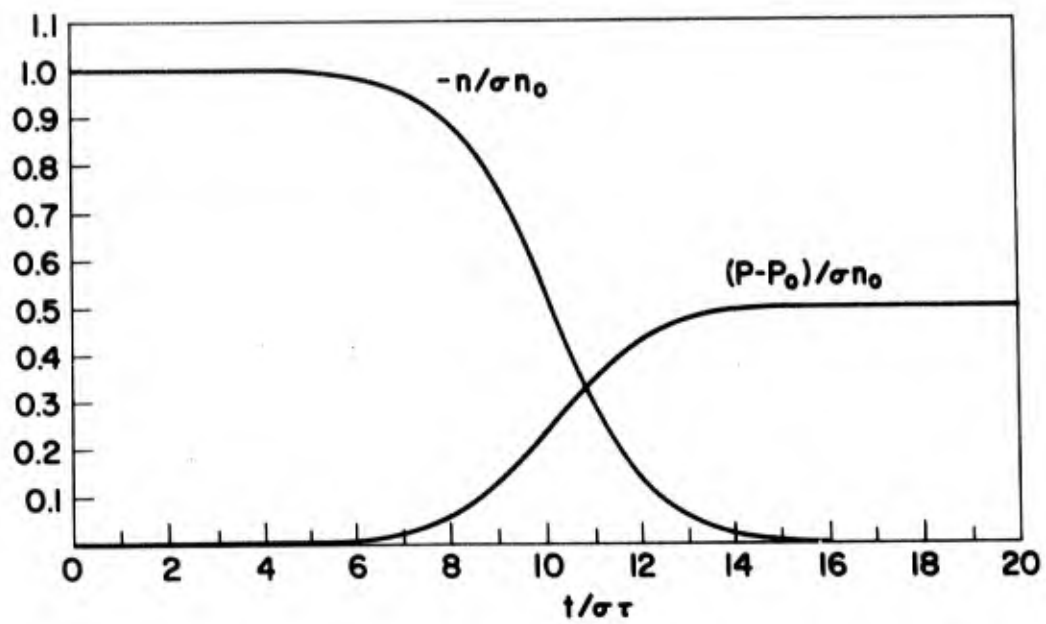


Figure 1 Theoretical avalanche relaxation curves, plotted as a function of $t/\sigma\tau$, for $T_1/\sigma\tau = 5 \times 10^4$.

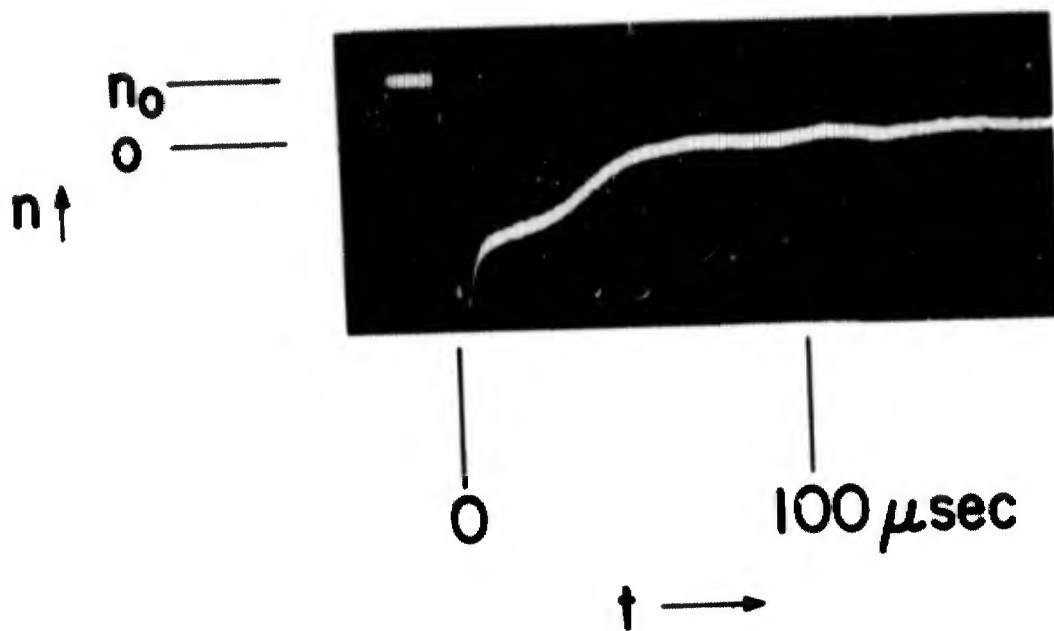


Figure 2 Experimental relaxation curve showing both $\Delta M = 2$ and $\Delta M = 1$ avalanches. Time scale $20 \mu\text{sec/cm}$ (r. f. probe).

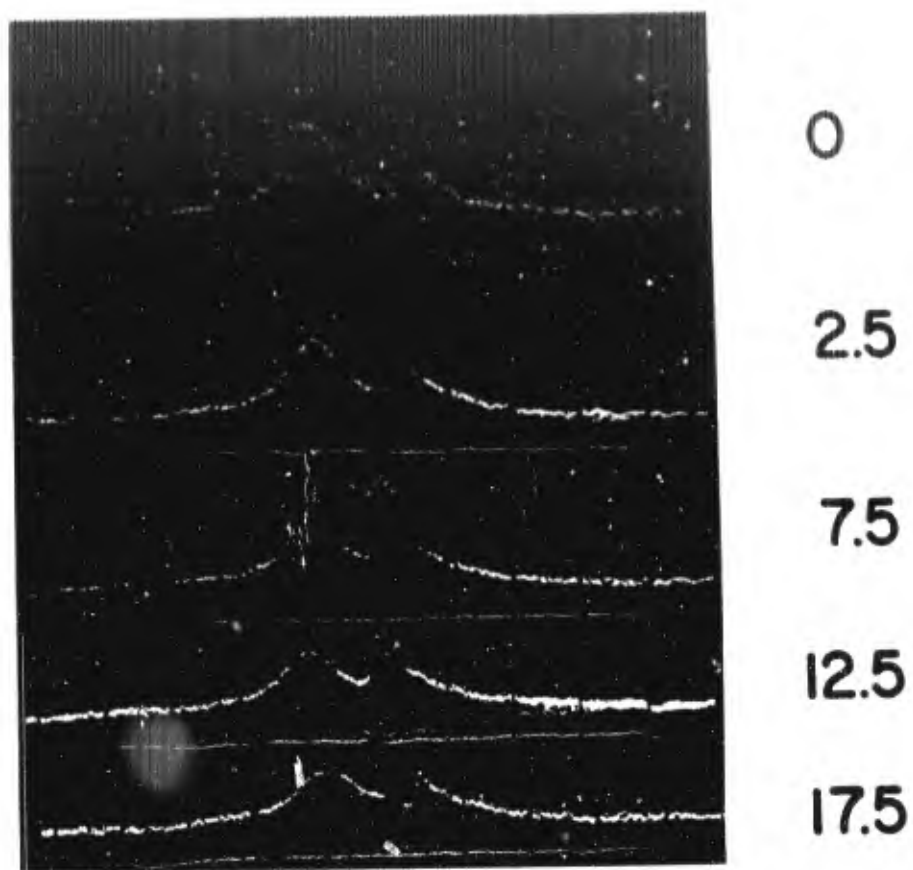


Figure 3 Ni^{2+} line shape for several delay times (in μsec) after incomplete rapid passage, obtained by sampling techniques as explained in text. The normal absorption line, as well as a zero-signal baseline, is also shown on each picture (ultrasonic probe).

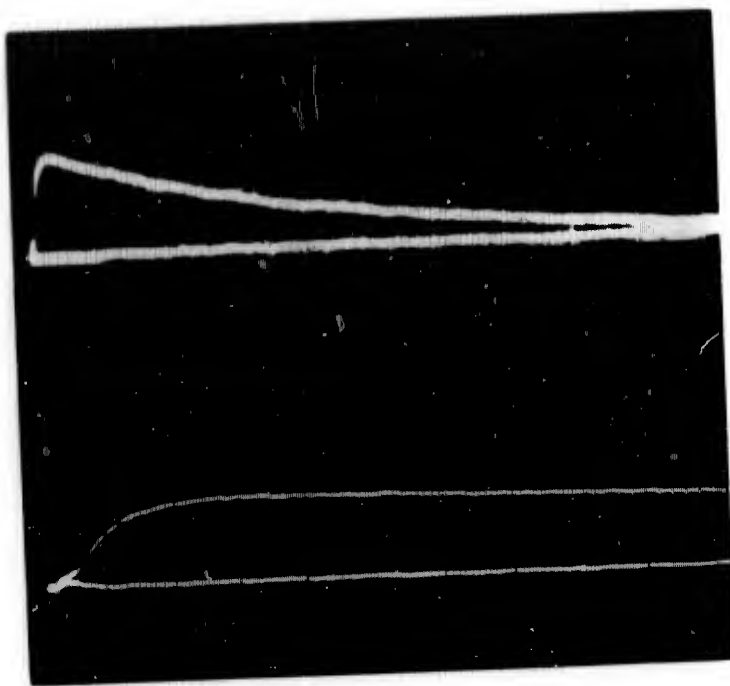


Figure 4 Oscilloscope photographs of detected phonon pulses. Lower photo: $10 \mu\text{sec}/\text{cm}$. Upper photo: $100 \mu\text{sec}/\text{cm}$.

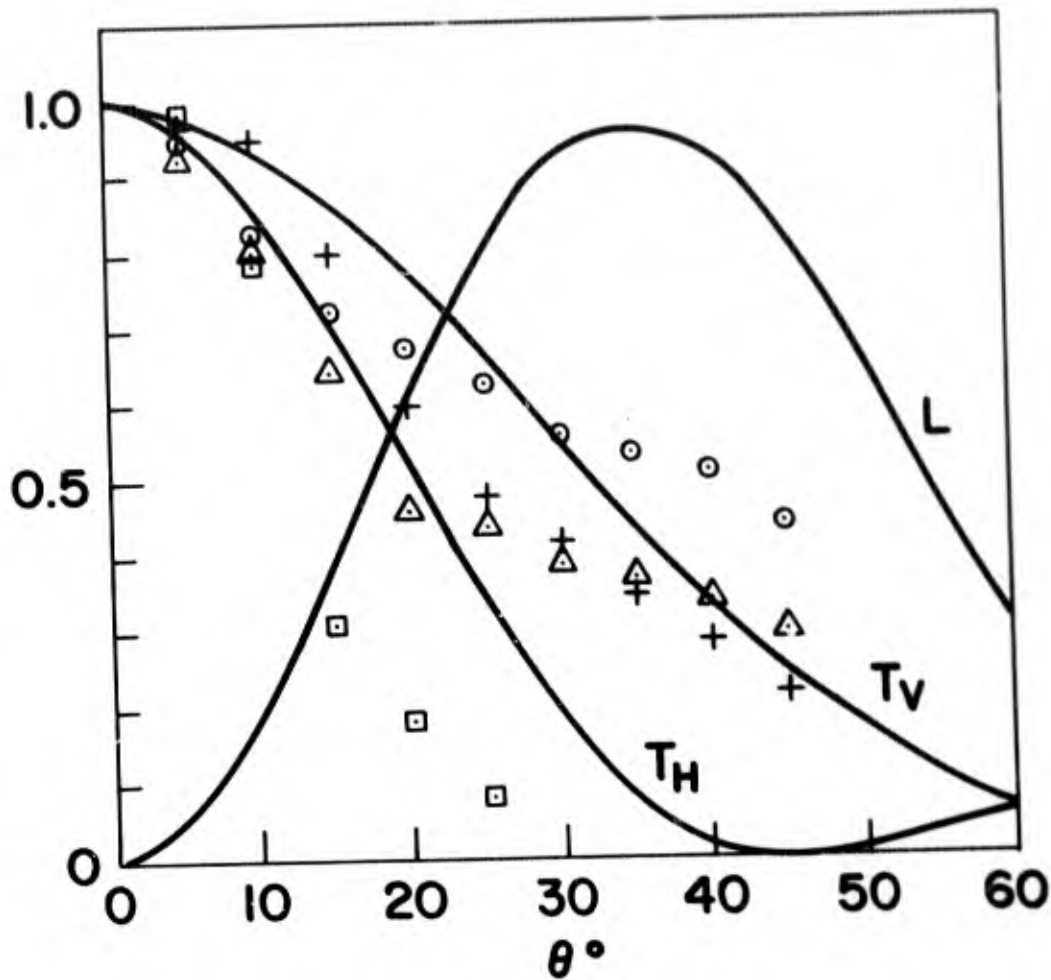


Figure 5 Relative measured intensities (points) for several runs, and theoretical detector sensitivities (curves) for waves propagating on $\langle 100 \rangle$. L, longitudinal polarization, T_V , transverse polarization normal to plane of rotation of magnet, and T_H , transverse polarization in the rotation plane, plotted as a function of θ , the angle between the magnetic field and propagation vectors. Experimental points normalized at $\theta = 0^\circ$. Points labelled by squares were taken under condition of relaxation in the presence of the strong microwave pulse.

II THE TEMPERATURE DEPENDENCE OF HEAT PULSE PROPAGATION IN SAPPHIRE

Data has been reported earlier on the propagation of heat pulses in quartz and sapphire at 3.8° and $\sim 8.5^{\circ}\text{K}$.¹ Other reports have since appeared on the propagation of heat pulses in sapphire and other solids.²⁻⁵ Such experiments furnish information on the energy velocity of phonons as well as on various phonon defect⁵ scattering processes. The effects of phonon-phonon scattering events on the shape of the heat pulse can also be investigated when such experiments are carried out at higher temperatures. A wavelike propagation of heat pulses⁶ (second sound) may result from a high rate of normal process events compared to all other scattering events. Additional references on the dynamic heat flow in crystals appear in a recent paper by Chester.⁷

We have extended our earlier work on single crystal z-cut sapphire to obtain heat pulse data as a continuous function of temperature up to 54°K . This is well above the temperature

($\sim 30^\circ\text{K}$) of the thermal conductivity maximum,⁸ the temperature near which a maximum number of N-process compared to U-process collisions should occur and therefore near which second sound is most likely to occur.

The findings of the present experiment are (1) the observed onset time of the arriving heat pulses for the longitudinal phonons is essentially constant for the temperature range $4\text{-}40^\circ\text{K}$ and for the transverse phonons this time is almost constant, increasing by only $\sim 5\%$ over this temperature range ; (2) as the temperature increases the amplitude of the sharp transverse pulse relative to the longitudinal pulse decreases ; also by 18°K appreciable phonon-phonon scattering is present which gives rise to an additional diffuse maximum at times substantially later than either the acoustic energy transport time or that expected for second sound ; (3) from 40°K - 54°K , no observable heat arrives at the acoustic velocity, but the heat arrives instead by diffusion at a very much later time in agreement with thermal conductivity results.

As before, a heat pulse was generated on one face of a z-cut sapphire crystal and detected on the opposite face. Light from a giant pulse ruby laser (half power width ~ 40 nsec) was absorbed in an evaporated alloy film ($\text{In}_{0.94}\text{Sn}_{0.06}$). With masks to define

the light beam, 0.4" and 0.1" diameter heat sources were available. The detector was an evaporated thin film of pure indium. It consisted of closely spaced 2 mil lines $\sim 2000 \text{ \AA}$ thick in a zigzag array covering .060" x .090". This film was used as a bolometer with ~ 20 ma bias current. The voltage change was proportional to incident heat pulse power. The small heat capacity of the detector provided a fast thermal response.^{9, 10} The sapphire crystals were supplied by the Valpey Crystal Co. with 1.00 and 0.50 cm lengths and 0.59 cm diameter.

The shapes of the received pulses at various temperatures are shown in Figs. 1 and 2 for the 1/2 cm crystal and the 0.4" heat source. The first pulse is caused by stray laser light reaching the detector directly. Its decay indicates that the response speed of the overall system is limited mainly by the electrical circuits to ~ 25 nsec. The velocities corresponding to the onset times of the transverse and longitudinal pulses are listed in Table I and are quite independent of temperature. These values are in good agreement with the energy velocities calculated from the phase velocities with the aid of calculations by Farnell.^{1, 11} The observed rise time of $\sim 0.2 \mu\text{sec}$ of the modes can be accounted for by the finite size of the heater and detector. At

the lowest temperatures, the detector response does not return to zero after the sharp pulses have passed as was reported previously.¹ This is a consequence of the high power input used and has been observed previously, but no detailed explanation can be given.

The observed decrease in the ratio of the unscattered transverse to longitudinal heat pulse amplitude with increasing temperature is consistent with the larger increase of the shear wave attenuation with temperature than the longitudinal attenuation as observed with 1 KMc ultrasonic waves.¹² The absolute peak heights are affected by the change in detector sensitivity with temperature,^{9, 10} but clearly less heat must arrive in the sharp pulses above 18°K since appreciable heat is scattered from the direct beam and arrives at a later time. The unexpected feature is that the sharp pulses are not continuously broadened and do not shift appreciably to later arrival times. Instead, the diffuse maximum due to scattered phonons appears at a considerably later time and gradually increases in height and in arrival time in the temperature range ~ 18° → 40°K. Little, if any, additional heat flow is found in the region between the sharp maxima and the broad maximum. The structure of the broad maximum at 38°K is shown in Fig. 2.

Above 40°K the unscattered modes were essentially absent, leaving only heat transport by diffusion. A thermal conductivity mean free path can be calculated (Table II) from the heat pulse data by using the special one dimensional solution¹³ for a δ function heat flux excitation at $x = 0$.

$$\Delta T \propto \frac{\Delta T_0}{\sqrt{t}} e^{-x^2/4\kappa t} \quad (1)$$

Here κ is the diffusivity of the sapphire and ΔT the temperature above ambient at a distance x from the excitation. Although Eq. (1) is not expected to hold exactly for a sample of finite length, it should be obeyed reasonably well especially for the initial stages of the diffusion pulse. A comparison of phonon mean free paths from heat pulse data using Eq. (1) evaluated at $\Delta T/\Delta T_0 = .25$ and those calculated from thermal conductivity ($l = 3K/\bar{Cv}$) data⁸ are in quite good agreement. (Here ΔT_0 is the maximum temperature reached by the detector.)

It might also be mentioned that for high input powers at the lowest temperatures an additional heat pulse arrival time is observed which corresponds to an echo at three times the onset time of the unscattered transverse mode. This pulse was only observable near 4.2°K. The disappearance of this echo at higher temperatures is related to the increase in the observed attenuation of the transverse mode already discussed.

Thus, the effects observed in the study of heat pulse propagation in sapphire at both the higher and the lower temperatures are as expected from the theory of diffusive and ballistic heat flow respectively. At the intermediate temperatures between $18^{\circ} - 40^{\circ}\text{K}$, the persistence of the sharp unshifted pulses while the heat flow is becoming mainly diffusive is rather unexpected since one might have expected a gradual broadening and shift of the sharp pulse into the more diffusive type of behavior. Instead, the sharp pulse persists even at temperatures where the bulk of the heat arrives considerably later due to diffusion. This may be related to a rather abrupt and unexpected difference in behavior of the lower frequency and higher frequency phonons comprising the heat pulse.

A possible explanation of these observations might be the following: The higher frequency phonons may suffer frequent large angle scattering processes (probably predominantly U-processes and perhaps some point defect scattering) and thus contribute to the broad maximum. The low frequency phonons may either be unscattered or suffer only small angle N-process collisions. These would directly interfere only slightly with the thermal current and heat pulse shape. The intermediate frequency phonons must then either be too few in number or their

rate of large angle N-process collisions must be too low to produce a significant contribution to the heat flow at the velocity corresponding to that expected for "second sound". It has recently been suggested that the N-process events may be predominantly small angle collisions.^{14, 15, 16} For such normal process collisions, second sound cannot be expected to occur, and, in fact, no indication of second sound or even of an approach to second sound is seen in the data.

The data for both the 0.4" diameter and the 0.1" diameter heat source show no essential difference. The larger heat source would be the more likely one for which second sound might be observed. The ratios of input pulse width to transit times in the 1/2 cm crystal were ~ 0.1 and 0.05 for the longitudinal and transverse pulses respectively. Thus most of the external conditions for this experiment were rather similar to those employed in the recent experiment on solid helium for which the observation of second sound has been reported.⁴ Even though there is not necessarily a direct conflict between these two results (since the role of phonon collisions may be quite different in the two materials), it would be of considerable interest to extend the solid helium results to lower temperatures to investigate the transition from the reported behavior to the expected ballistic flow at the ordinary sound velocity.

This work was done in collaboration with A. H. Nethercot.

REFERENCES

1. R. J. von Gutfeld and A. H. Nethercot, *Phys. Rev. Lett.* 12, 641 (1964).
2. J. M. Andrews and M. W. P. Strandberg, *Proc. IEEE* 54, 523 (1966).
3. J. B. Brown, D. Y. Chung and P. W. Matthews, *Physics Lett.* 21, 241 (1966).
4. C. C. Ackerman, B. Bertram, H. A. Fairbank and R. A. Guyer, *Phys. Rev. Lett.* 16, 789 (1966).
5. R. J. von Gutfeld and A. H. Nethercot, *International Low Temperature Physics Conf. LT9* (Plenum Press, New York, 1965), pp. 1189-1192.
6. J. C. Ward and J. Wilks, *Phil. Mag.* 42, 314 (1951).
7. M. Chester, *Phys. Rev.* 145, 76 (1966).
8. R. Berman, *Z. für Phys. Chem. (Neue Folge)* 16, 10 (1958).
9. R. J. von Gutfeld, A. H. Nethercot, Jr., and J. A. Armstrong, *Phys. Rev.* 142, 436 (1965).
10. R. J. von Gutfeld and A. H. Nethercot, Jr., *J. Appl. Phys.*, (to be published Sept. 1966).
11. G. W. Farnell, *Can. J. Physics* 39, 65 (1961).
12. J. de Klerk, *Phys. Rev.* 139, A 1635 (1965).
13. H. G. Carslaw and J. C. Jaeger, *Conduction of Heat in Solids*, Oxford, Clarendon Press, 1947, p. 57.
14. S. Simons, *Proc. Phys. Soc.* 82, 401 (1963).
15. H. J. Maris, *Phil. Mag.* 9, 901 (1964).
16. I. S. Ciccarello and K. Dransfeld, *Phys. Rev.* 134, A 1517 (1964).

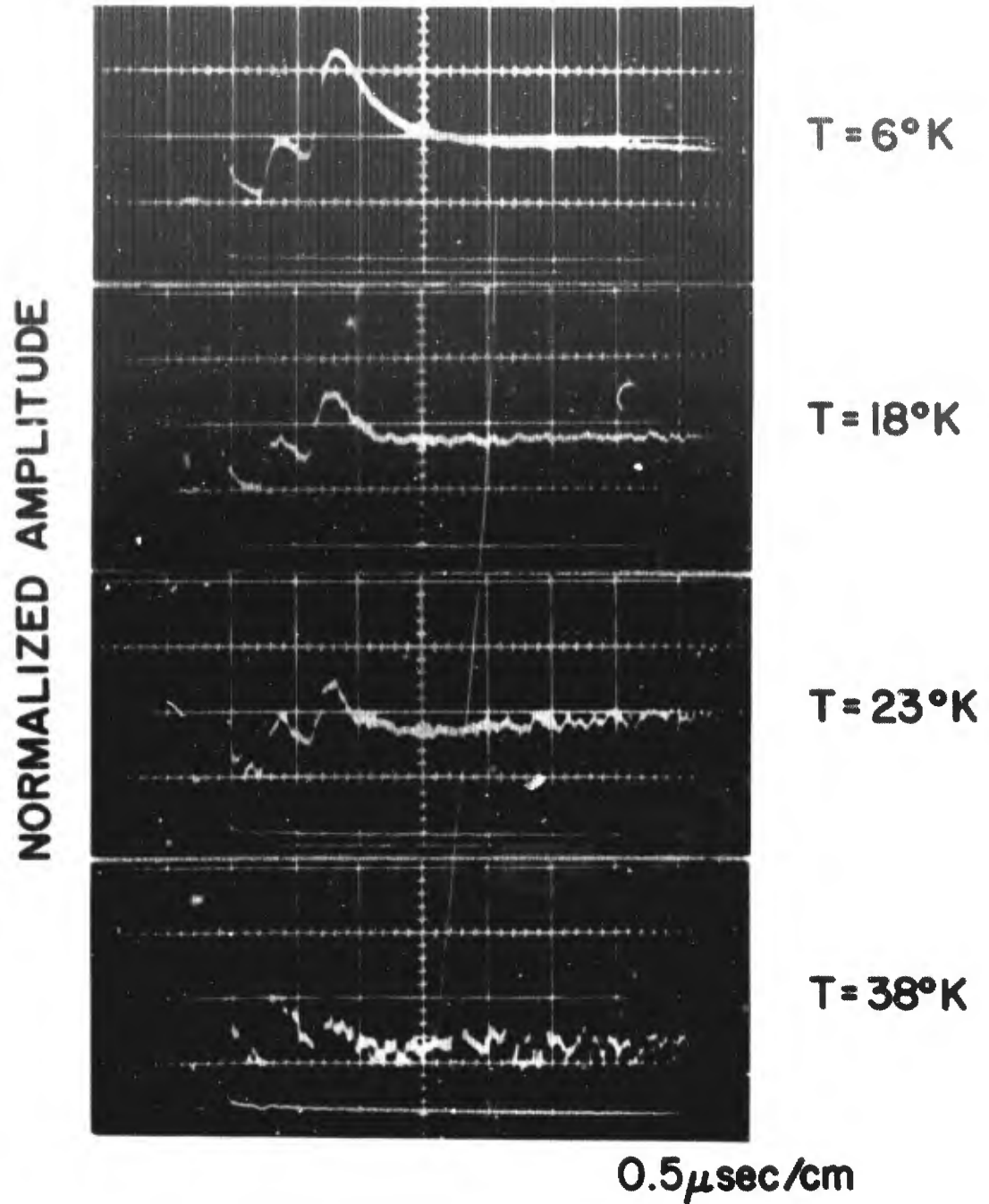
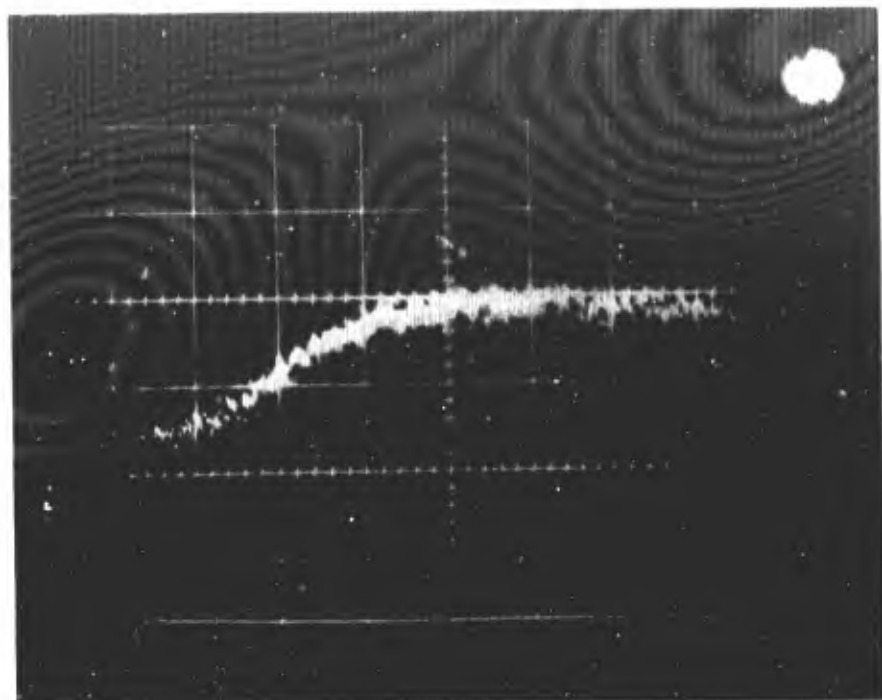


Figure 1 Observed heat pulses (upper trace) after propagating through a 1/2 cm sapphire crystal at four different temperatures. The initial pulse is due to laser light falling directly on the detector; the second and third pulses represent heat arriving with the longitudinal and transverse phonon velocities. The lower trace in these figures is the direct response of a phototube to the laser light. The time scale is 0.5 μ sec/cm (major division).



$T = 38^{\circ}\text{K}$

$5\mu\text{sec/cm}$

Figure 2 The heat pulse observed at 38°K , indicating a broad temperature maximum characteristic of heat flow by diffusion.

III DETECTION OF ULTRASOUND USING THIN FILM BOLOMETERS

A number of experiments have been performed at 9.2 GHz on AC and x-cut quartz crystals using In-Sn thin film detectors. The μ -wave detection scheme is similar to the method used in the detection of heat pulses except that here a narrow band of frequencies impinges on the bolometer. The advantage of this type of detection over the standard μ -wave ultrasonic detection is that parallelism of the end faces of the crystals should not be important if the detector responds only by a change in its resistance due to heating. For such situations the phase of the incident μ -wave phonons becomes unimportant. "Beating" effects observed in ultrasonic echo patterns would also not be expected. Therefore, such a detector should be capable of detecting incoherent μ -wave phonons.

The preliminary experiments to be reported were carried out at temperatures in the range 1.8-3.8^oK (a magnetic field was used below 3.8^oK) using In-Sn films of thickness $\sim 2000 \text{ \AA}$ evaporated onto one end of AC and x-cut single crystal quartz rods. The films covered $\sim 10\%$ of the end face area. Experiments were also made in the range 4.2-12^oK using pure indium film detectors. However, above 4.2^oK, echoes were observable only in the AC cut quartz. The cavity, sample and detector

arrangement are shown in Fig. 1. For temperatures below 4.2°K the entire assembly was immersed in liquid helium.

Some of the observed echo patterns using the bolometer are shown in Fig. 2. For comparison the μ -wave phonon echoes detected by standard electromagnetic techniques are also shown. If L equals the crystal length ($L = 1.5$ or 1.75 cm in these experiments) and v the phonon velocity, then the echoes detected by the film occur at times equal to nL/v , where n equals 1, 3, 5 etc. Those detected electromagnetically occur at even integers n ($n \neq 0$). The displacement in echo patterns by l/v is due to the relative location of the two detectors (Fig. 1).

A number of features of the bolometer echoes are quite unexpected and not well understood. The most striking of these is the rapid attenuation which greatly reduces the number of echoes observed bolometrically compared to electromagnetic detection. Furthermore the attenuation of successive echoes is not exponential: a modulation effect is observed, similar to that observed in phonon assisted tunneling experiments. Thus, for example, it can be observed that the third echo is actually larger than the preceding one in the lower trace of Fig. 2b. This is quite unexpected for a detector of incoherent phonons.

The theoretical attenuation in the metal film can be calculated

using the free electron model of Pippard. For our alloy films, if one assumes the electron mean free path, l_e , to be $\sim 400 \text{ \AA}$, for the phonon wavevector $q = \frac{2\pi}{\lambda}$ corresponding to 9.2 KMc one obtains $ql_e \sim 2.0$. The transverse and longitudinal amplitude attenuation for $ql_e \sim 1$ in the normal state of a metal are given approximately by

$$a_t = \frac{2}{3\pi} \frac{Nm v_o \omega}{\rho_o u_s^2} \quad (1a)$$

$$a_l = \frac{\pi}{12} \frac{Nm v_o \omega}{\rho_o u_l^2} \quad (1b)$$

in units of cm^{-1} . Here N is the number of free electrons/volume, m the electron mass, v_o the Fermi velocity, ω angular frequency of the μ -wave, ρ_o the density of the metal and u_l the phonon velocity. For values of the phonon velocity in the $[001]$ direction which is very approximate for this experiment because the metal film is not single crystal, one obtains theoretical values of $a_t = 600 \text{ cm}^{-1}$ and $a_l = 200 \text{ cm}^{-1}$. For longitudinal phonons this is an order of magnitude smaller than the observed value of $a \approx 4 \times 10^3 \text{ cm}^{-1}$ found by taking the slope of Fig. 3. No explanation can be given so far for this abnormally large attenuation.

An attempt to measure the difference in attenuation between

a superconductor and normal metal was made by covering the entire end face of a quartz crystal with $\sim 2000 \text{ \AA}$ In-Sn film. If the attenuation were really as large as the bolometer indicates a difference should be observed in the electromagnetically detected echoes in the normal and superconducting states. However at 1.5°K no difference was observed. This indicates that the attenuation for such a thin film is very small in the normal state and even smaller in the superconducting state, so that no effect was observed.

Other features of the data which are not well understood are the dependence of the height of bolometrically observed echoes on input μ -wave power, and in certain cases the pulse shape of the individual echo. Figure 3 is a plot of successive echo amplitudes at different input powers for bolometer detection in AC cut quartz rod. A change in modulation pattern is apparent though an attenuation of $\approx 1.4 \text{ DB}$ can be measured between many successive echoes.

Though the effects observed here are not well understood, it would appear from the similarity of the effects observed in the intermediate and normal states of the metal, (Fig. 2a, b and Fig. 2c respectively) that the peculiarities cannot be ascribed to the superconducting properties of the metal. It is also evident

that this type of detection is not useful as an incoherent μ -wave phonon detector where absolute attenuation measurements are required. However the present type of investigation may lead to a new insight on the ultrasonic attenuation in metals.

REFERENCES

1. R. J. von Gutfeld and A. H. Nethercot, *Phys. Rev. Lett.* 12, 641 (1964).
2. R. J. von Gutfeld and A. H. Nethercot, *J. Appl. Phys.* 37, 3767 (1966).
3. E. Lax and F. L. Vernon, Jr., *Phys. Rev. Lett.* 14, 256 (1965).
4. B. Abeles and Y. Goldstein, *Phys. Rev. Lett.* 14, 595 (1965).
5. R. Morse, *Progress in Cryogenics* (1960).

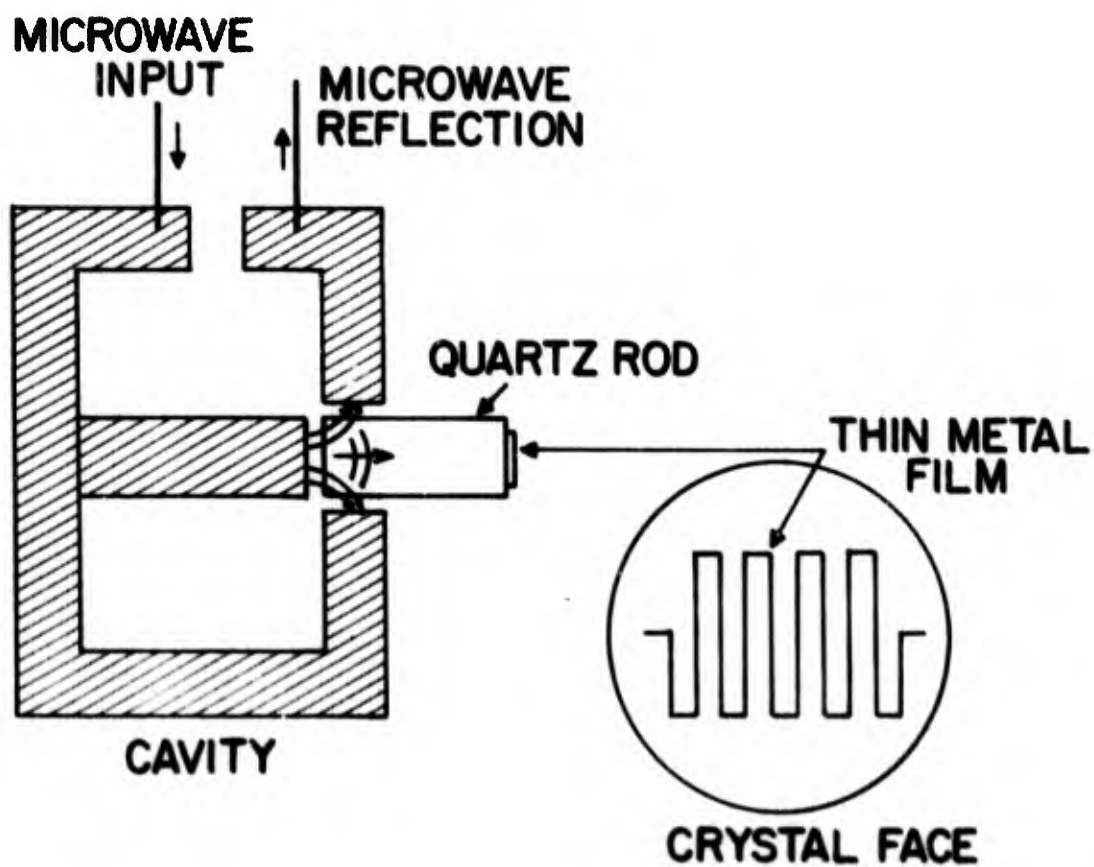


Figure 1 Schematic view of the microwave cavity and quartz rod with an evaporated thin film detector on one end of the rod.



↳ \sphericalangle $5\mu\text{sec/cm}$



↳ \sphericalangle $10\mu\text{sec}$



↳ \sphericalangle $5\mu\text{sec}$

Figure 2 (a) Echoes observed (lower trace) by an In-Sn detector at -2.1°K from 1.75 cm length x-cut quartz crystal. Some evidence of transverse modes is also present. The upper trace is the detection of the same echoes by standard electromagnetic techniques. (b) Echoes (lower trace) from AC quartz (1.5 cm length) at 2.9°K by bolometer detection (In-Sn) and (upper trace) electromagnetic detection. (c) Echoes (lower trace) observed in AC quartz (1.5 cm length) using pure In film detector at -9°K . The upper trace is the detection by standard electromagnetic techniques.

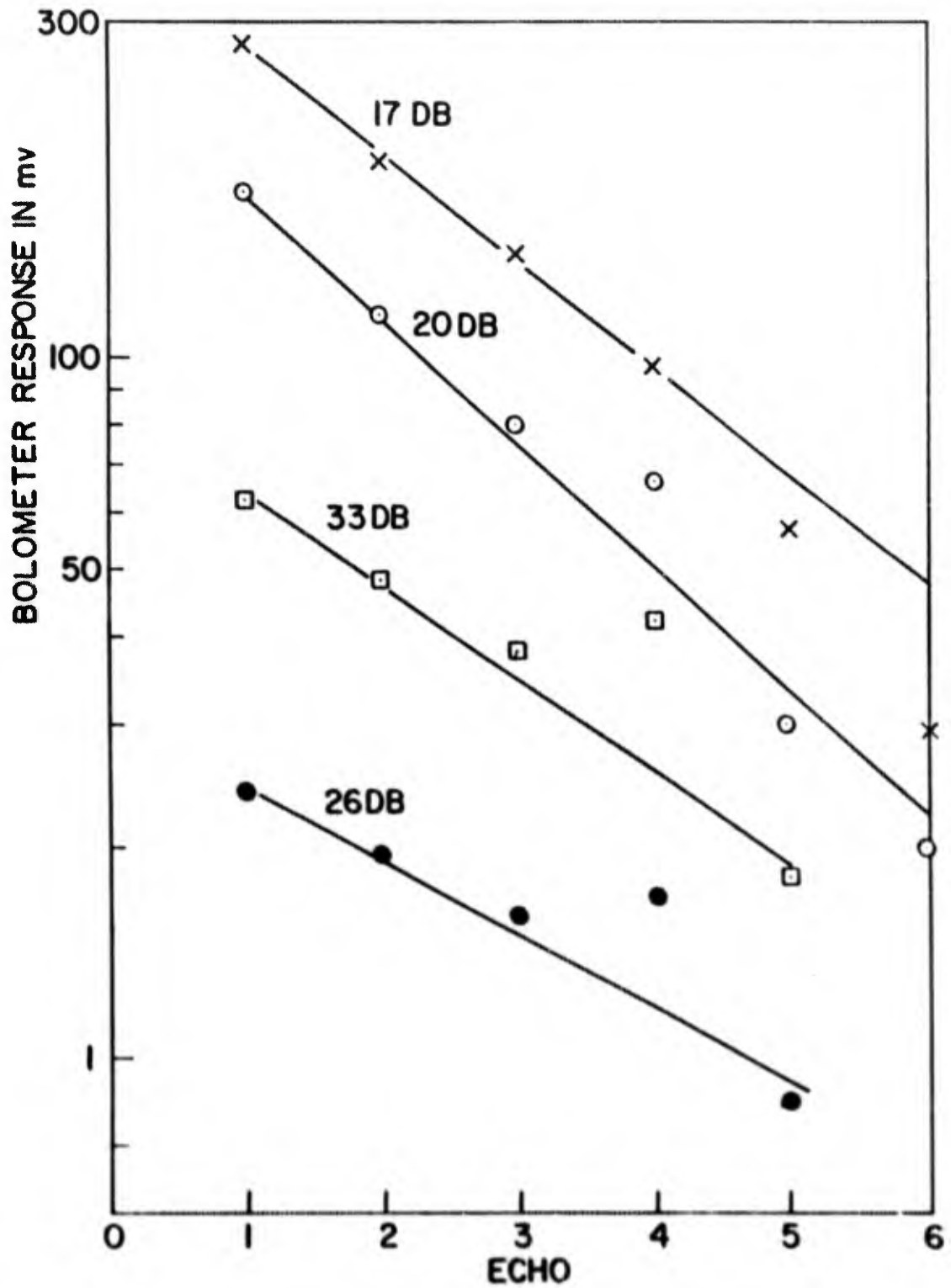


Figure 3 Typical echo amplitude observed in AC quartz by means of a thin film detector for various levels of input microwave power.

SUMMARY OF WORK UNDER CONTRACT DA36-039AMC-02280(E)

I. PHONON-PHONON INTERACTION

To the extent that the interatomic forces in a crystal are harmonic, phonons are non-interacting modes of vibrations of the lattice. The anharmonic terms in the lattice potential lead to coupling of the phonons. We have studied phonon-phonon interactions in several ways: (a) the interaction of three microwave phonons, which can result in phonon amplification, (b) interaction of ultrasonic phonons with thermal phonons, which leads to ultrasonic phonon attenuation, (c) interactions among several thermal phonons, observed in heat pulse propagation, (d) the transmission of heat from metal films to insulating substrate, (e) the occurrence of displacive ferroelectricity and anti-ferroelectricity. This work is summarized below.

A. Interactions of Three Microwave Phonons

Nonlinear interactions (three phonon processes) among collinearly propagating acoustic waves were extensively investigated. Parametric up-conversion and amplification as well as second harmonic generation were all observed in MgO. In addition to studies of the dynamics of these processes, the third order elastic constants in a variety of materials were determined from quantitative measurements of the inter-

action strengths. A means of introducing selective dispersion by the use of paramagnetic impurities was developed. The dispersion was used to suppress the generation of undesirable frequency components. Without it, parametric amplification would not have been possible.

The experimental geometry is shown in Fig. 1. It consists of the usual re-entrant cavity with the addition of a rectangular cavity, positioned so that the bonded surfaces of the crystals lay in the maximum microwave electric field, with the **MgO** crystal extending through the back of the cavity. The x-cut quartz transducers were 1.75 cm long and 3 mm in diameter. They were bonded to **MgO** crystals of the same diameter and ~ 1 cm long with GE-7031 resin.

In the harmonic generation experiments, only the re-entrant cavity was used to generate a single input. For the experiments utilizing two acoustic inputs the second was generated at the bonded surface of the quartz. The efficiencies of generation and detection in the rectangular cavity were ~ 8 dB lower than in the re-entrant cavity. However, this method of obtaining two acoustic inputs obviates the necessity for two bonds, the use of which is particularly disadvantageous

at microwave frequencies.

For the up-conversion case, i. e., the generation of the sum frequency wave $\omega_u = \omega_s + \omega_p$ from a low power signal at a frequency ω_s and a strong pump at frequency ω_p , the theoretically predicted decrease in the low power signal strain amplitude is, for small propagation distances, x ,

$$\Delta e_s / e_s = \frac{1}{2} \left(\frac{A_{111}}{4C_{11}} \right)^2 e_p^2 \omega_s \omega_p x^2 / v^2$$

Here A_{111} is a third order elastic constant, C_{11} is a second order elastic constant, e_s and e_p are the signal and pump strains, and v the velocity. An experimental result showing this behavior is given in Fig. 2.

For harmonic generation the theoretically predicted harmonic (e_2) and fundamental (e_1) strain amplitudes behave as follows:

$$e_2(x) = e_1(0) \tanh \beta x$$

$$e_1(x) = e_1(0) \operatorname{sech} \beta x$$

$$\text{where: } \beta = \frac{1}{2} (A_{111} / 4C_{11}) (\omega_1 \omega_2)^{1/2} e_1 / v$$

The theory predicts in the limit of $e_1 \omega x$ becoming very large, all of the fundamental is converted irreversibly to second harmonic. This result has been experimentally confirmed out to ~90% power conversion as shown in Fig. 3.

Second harmonic signals have also been directly observed (See Quarterly Report No. 2) in experiments in which one of the cavities was tuned to an x-band frequency and the other to the harmonic at Ku band.

For the experiments on amplification the pump cavity was tuned to 16.5 GHz. The expected signal strain variation is,

$$e_s(x) = e_s(0) \cosh \alpha x$$

if the pump amplitude (e_p) is assumed constant over the whole propagation path. Here,

$$\alpha = (A_{111}/4C_{11}) (\omega_s - \omega_p)^{1/2} e_{p/v}$$

The experimental results, Fig. 4, show the effect of pump depletion.

Values of $|A/C|$ were determined for longitudinal wave propagation on several crystallographic axes in several materials. They are summarized in Table 1.

These topics are discussed in detail in Quarterly Progress Reports 1, 2 and 4.

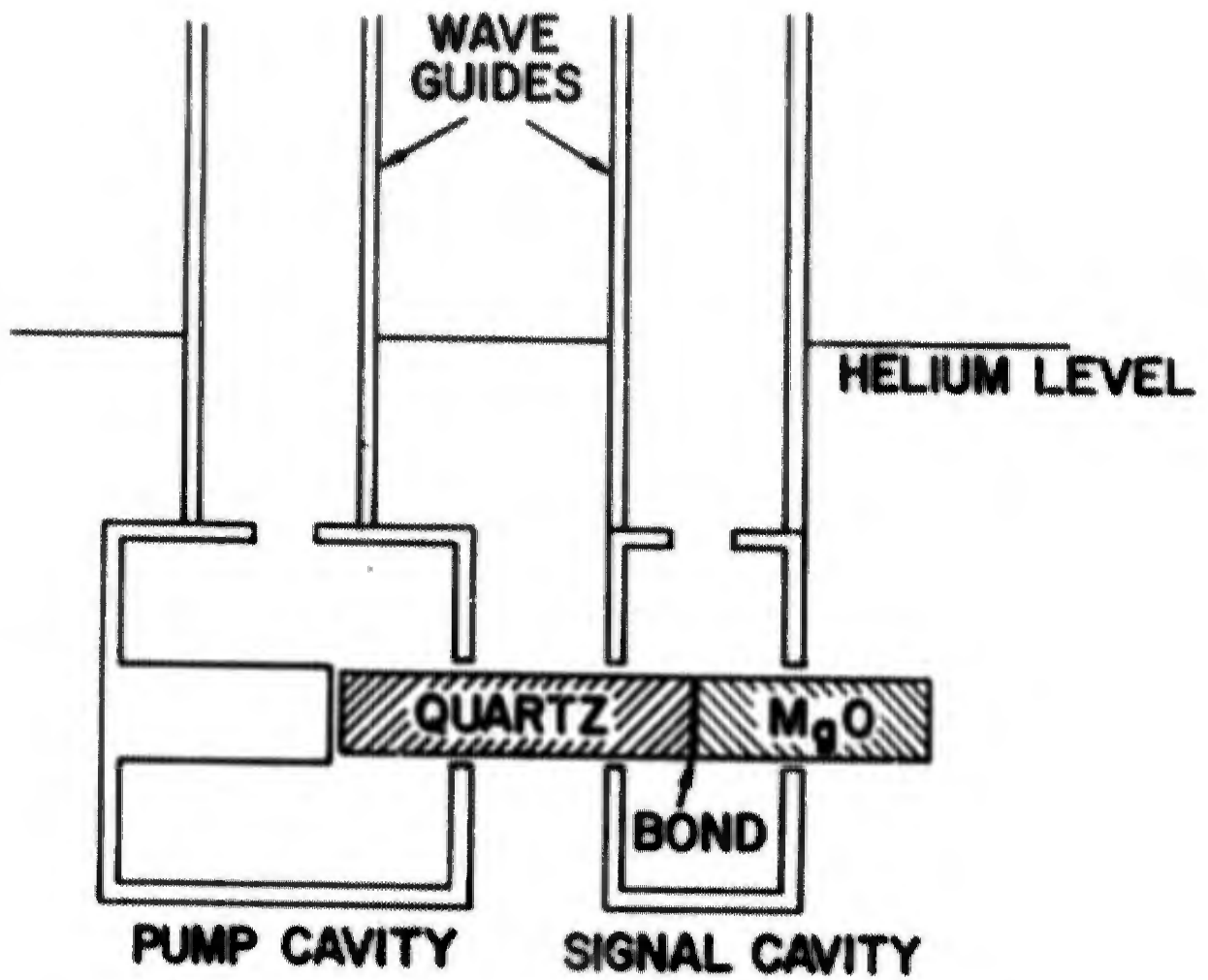


Figure 1 Schematic diagram showing ultrasonic drive cavities and crystal arrangement.

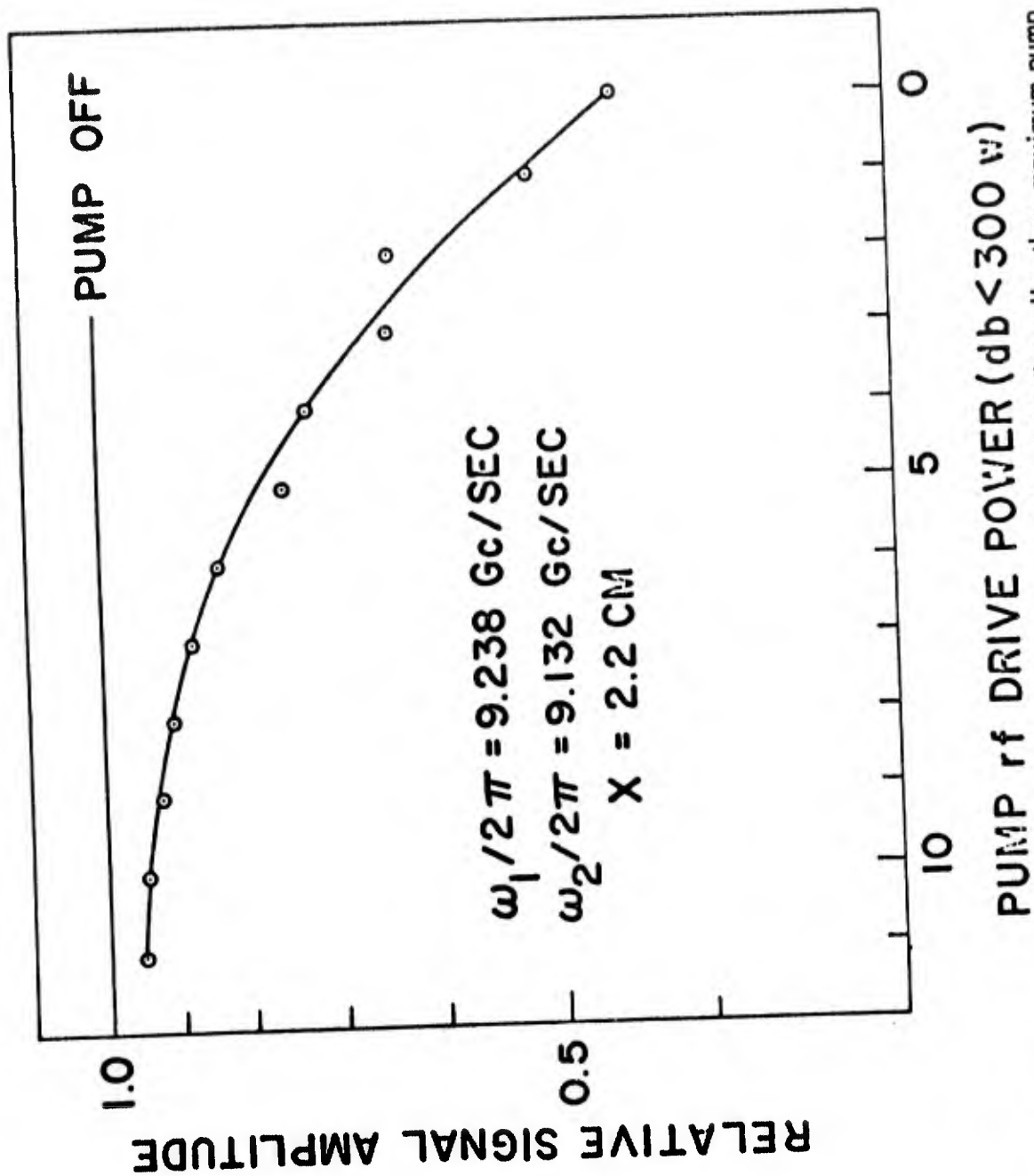


Figure 2 Signal amplitude vs. pump power for input signal level 20 db smaller than maximum pump input level.

2nd HARMONIC $\nu = 9.110 \text{ Gc/s}$
 e/e_0 vs e_0

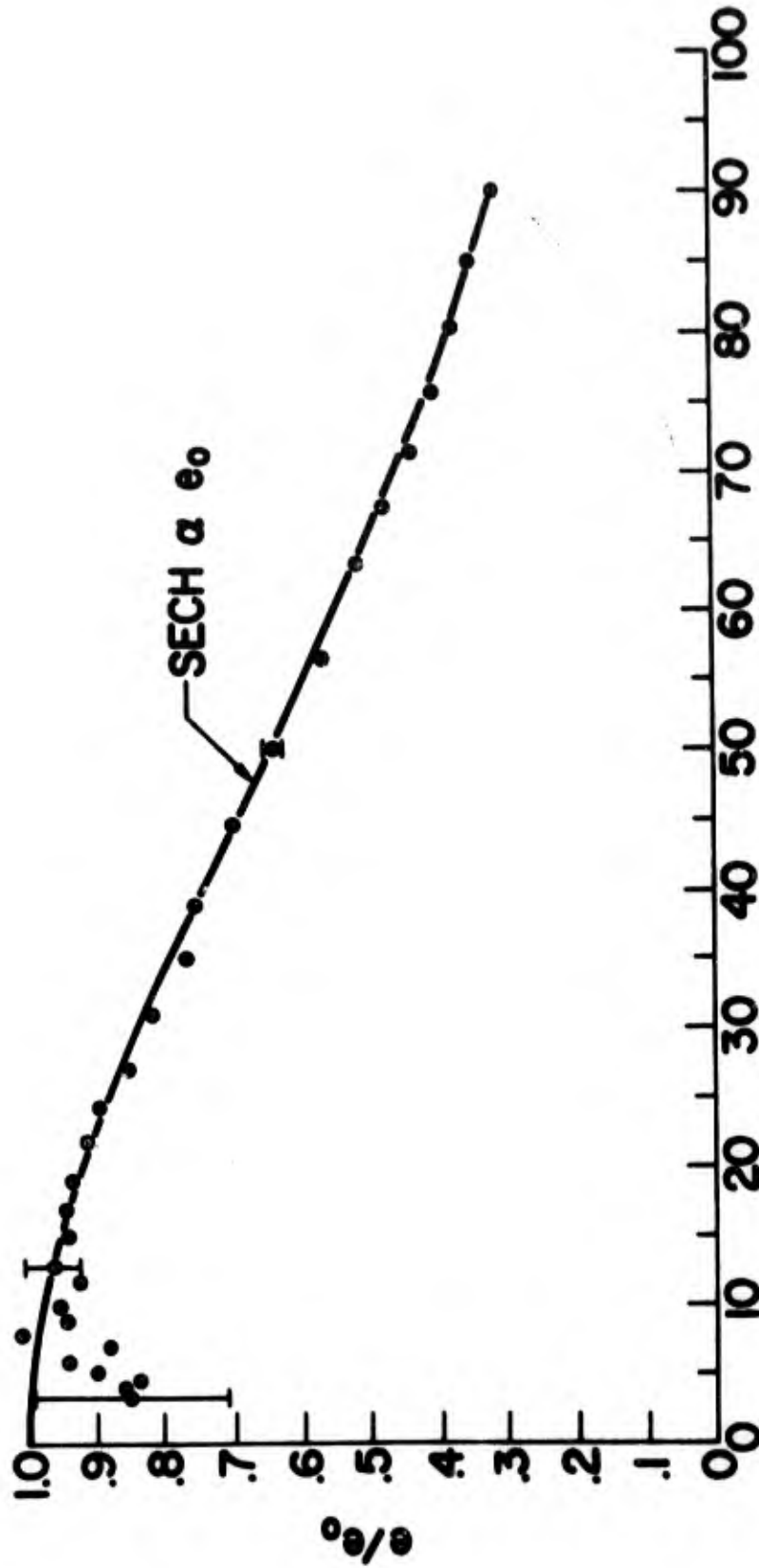


Figure 3 Normalized fundamental amplitude plotted against input fundamental amplitude.

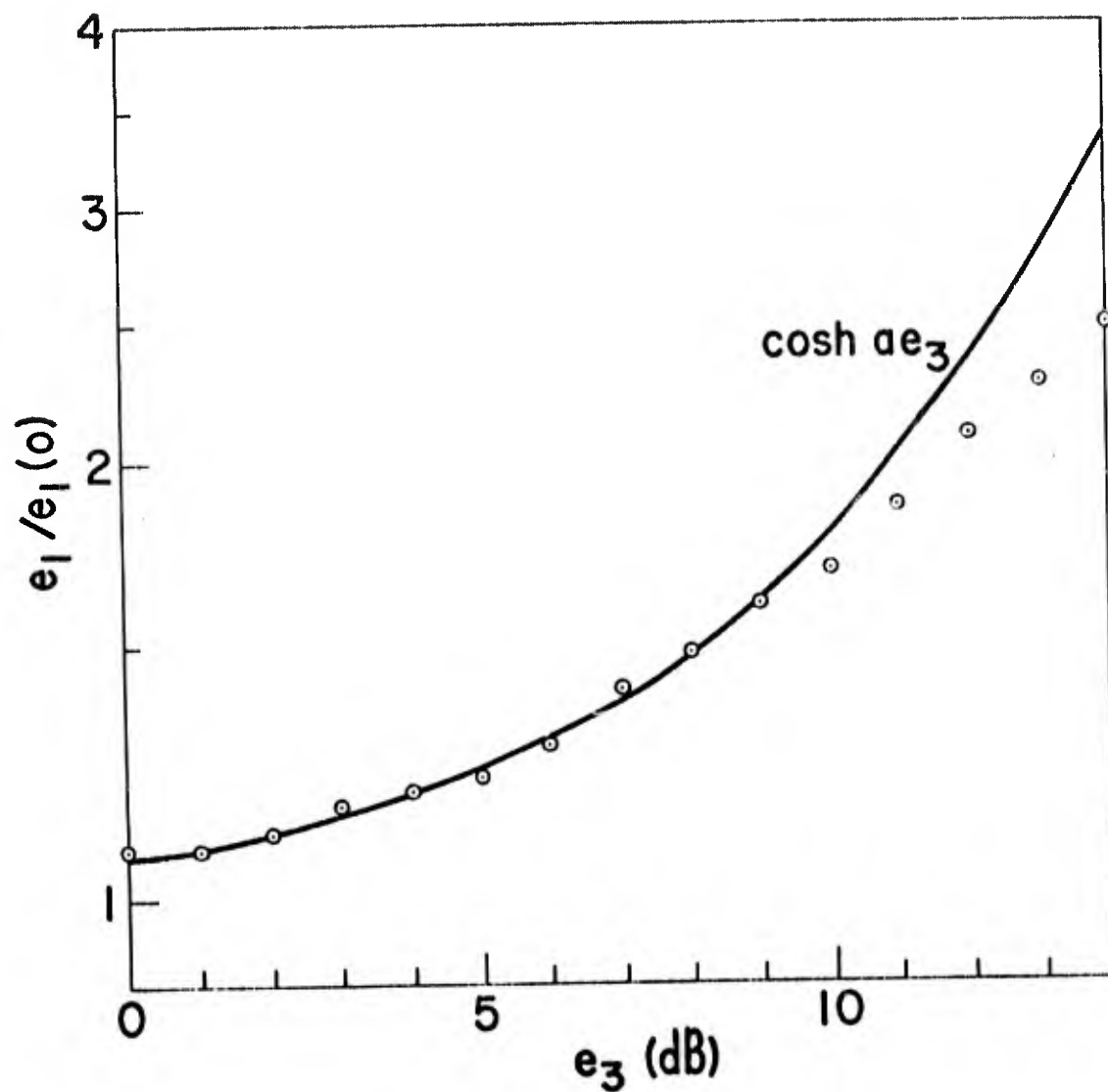


Figure 4 Signal amplitude measurements vs. pump amplitude, and theoretical curve, showing effect of pump energy depletion in a 2 cm crystal. a is an adjusted proportionality constant.

Table 1

Crystal	Axis	A/C
MgO	100	8.7 ± 0.9
	110	3.5 ± 0.4
	111	$0.4 \pm (50\%)$
CaF ₂	100	$6 \pm (50\%)$
	110	$10 \pm (50\%)$
Al ₂ O ₃	(a)	< 1
	(c)	< 1
α - Quartz	(x)	< 0.2
	(z)	$5 \pm (50\%)$

B. 1) General Theory Ultrasonic Attenuation in Insulators

The attenuation of an acoustic phonon by its interaction through the anharmonic lattice potential with thermal phonons depends on the width (inverse lifetime) Γ of the thermal phonon states when $\omega_k \Gamma^{-1} \lesssim 1$, where $\omega_k / 2\pi$ is the acoustic frequency. The well-known result for the region $\omega_k \Gamma^{-1} \ll 1$, originally derived by Akhieser, is $\Gamma(\omega_k) \propto \gamma^2 \omega_k^2 T c(T) \Gamma_T^{-1}(\omega)$ for $\omega = kT$ where γ is Gruneisen's constant, $c(T)$ is the lattice specific heat, $\Gamma_T(\omega)$ is the frequency-dependent width at temperature T ,

and we have taken T less than the Debye temperature θ_D . It was shown by a Green's function method that the Akhiezer result is valid only when the dominant scattering mechanism for thermal phonons gives rise to a weak frequency dependence of $\Gamma_T(\omega)$, e.g., normal three-phonon processes. On the other hand, when the scattering mechanism gives rise to a strong frequency dependence of $\Gamma_T(\omega)$, i.e., point defect scattering, we found a result for the acoustic attenuation which differs from the Akhiezer formula and which reflects the fact that the acoustic phonon now interacts most strongly with thermal phonons whose energy is considerably below kT . Also our theory provides a unified treatment for the entire range of values of the thermal-phonon lifetime.

The general result for the attenuation of a transverse acoustic phonon for T below the Debye temperature θ_D was found to be:

$$\alpha(\omega_\kappa) = \frac{\omega_\kappa}{32\pi^2 \rho^3 v_t^2 v_l^8} [A_{t,l,l}]^2 \int_0^\infty -\omega^4 \frac{\partial N(\omega)}{\partial \omega} \times \left[\tan^{-1} \frac{\omega_\kappa(r-1)}{\Gamma_T(\omega)} + \tan^{-1} \frac{\omega_\kappa(r+1)}{\Gamma_T \omega} \right] d\omega, \quad (1)$$

where $N(\omega)$ is the Bose-Einstein distribution function at T , r is the ratio v_l/v_t and $[A_{t,l,l}]^2$ represents the appropriate

average of the third order elastic constants over the angle between acoustic and thermal phonon. In the region $\omega_k \Gamma_T^{-1}(kT) \gg 1$, Eq(1) reduces to the Landau-Rumer result which is independent of the thermal phonon lifetime,

To examine the region $\omega_k \Gamma_T^{-1}(kT) \ll 1$, we characterize an arbitrary thermal phonon scattering mechanism by its frequency dependence.

$$\Gamma_T(\omega) = S_T \omega^n,$$

where n is an integer. For three-phonon normal processes $n = 1$, whereas for three-phonon umklapp processes $n = 2$, and for random scattering by point defects $n = 4$. One finds that for scattering mechanisms where $n < 3$, the main contribution to the integral of (1) comes from thermal phonons with frequency $\sim kT/h$, and one recovers the Akhieser result. When $n \geq 3$ one finds that the integrand of Eq. (1) has a maximum at a thermal phonon frequency ω considerably below kT/h given by $\omega_k \Gamma_T^{-1}(\omega) \sim 1$, so that thermal phonons below kT/h contribute most strongly to the attenuation. This leads to a different form for the attenuation when $n \geq 3$ which is given by

$$\begin{aligned}
 \alpha(\omega) = & \frac{\omega_{\kappa}}{32\pi^2} \frac{(kT)^4 [A_{t,l,l}]^2}{\rho^3 v_t^2 v_l^8} \\
 & \times \left\{ f_n \left[\frac{\omega_{\kappa}(r-1)}{\Gamma_T(kT)} \right] + f_n \left[\frac{\omega_{\kappa}(r+1)}{\Gamma_T(kT)} \right] \right\}
 \end{aligned} \tag{2}$$

where

$$f_n(\alpha) = \int_0^{\infty} y^4 e^y (e^y - 1)^{-2} \tan^{-1}(\alpha/y^n) dy.$$

Since we are considering the region $\omega_{\kappa} \Gamma_T^{-1}(kT) \ll 1$ we may evaluate $f_n(\alpha)$ explicitly.

$$\begin{aligned}
 f_n(\alpha) & \approx \alpha/6 \ln \alpha^{-2}, \quad n = 3 \\
 & \approx \frac{1}{3} g_n \alpha^{3/n}, \quad n \geq 4,
 \end{aligned}$$

where g_n is a numerical constant. These results show that when $n \geq 3$ the temperature and frequency dependence of the attenuation differ from the Akhieser form. For example for random scattering by point defects we find from Eq. (2) a linear dependence on T and a $\omega_{\kappa}^{7/4}$ frequency dependence. Point defect scattering is an important process in many materials. For example, in Ge it predominates near the thermal conductivity maximum.

We obtained similar results for the longitudinal wave by evaluating this collinear process $l+l \rightarrow l$, and recalling that

this process is allowed in spite of dispersion due to the finite lifetime of thermal phonons. Thus evaluating the collinear process we find the attenuation to be given by Eq. (1) with the subscript t replaced by the subscript l so that $r = 1$. This gives the same frequency and temperature dependence for both transverse and longitudinal acoustic attenuation. Also, although we have only obtained explicit results for $kT < k\theta_D$ we may include high temperatures by replacing the upper limit in the integral of Eq. (1) by $k\theta_D/h$. Then we again obtain the Akhieser result only for $n < 3$, whereas for $n \geq 3$ the integral of Eq. (1) must be evaluated explicitly for each scattering mechanism.

B. 2) Effect of Anisotropic Anharmonicity on Ultrasonic Attenuation in Insulators

A classical calculation of the attenuation of longitudinal waves due to three-phonon interactions with thermal phonons was presented in Quarterly Report No. 4. The results of this calculation were not different from those derived in the more usual quantum mechanical perturbation treatment. However, it appeared that the classical formalism was more easily adaptable to the situation where the crystal anharmonicity is anisotropic, and a calculation for this case was presented in Quarterly Report No. 10.

In previous formulations of the theory the parameter expressing the lattice anharmonicity had been taken as a generalized Grunelsen constant or average of third order elastic constants. It was shown that the attenuation of longitudinal waves (and of transverse waves propagating in certain crystallographic directions) is primarily due to collinear three phonon interactions involving two thermal phonons. In the range of temperatures, T , for which $\omega T \gg 1 \gg (1 - \beta) \omega T$ (where $\omega/2\pi$ is the acoustic frequency, T is the thermal phonon relaxation time and β is the ratio of thermal to acoustic phonon velocities) these calculations predict an ωT^4 dependence of the attenuation. Temperature dependences varying as T^n ($n > 4$) are predicted at still lower temperatures where $(1 - \beta) \omega T > 1$ and the energy uncertainty is not large enough to overcome the effects of dispersion. The theory has been successful in explaining the experimentally observed attenuation in many instances. On the other hand, in many other cases (see below) theory and experiment are at variance.

Our calculation showed that when the tensor properties of the anharmonicity are included in the theory, the resulting frequency and temperature dependences of attenuation are strongly dependent upon the degree of anisotropy of the tensor

components. This type of anisotropy can also exist in solids which are elastically isotropic in the usual (second order) sense and in the interest of brevity we consider these materials only. We also restrict the discussion to the case of longitudinal wave attenuation due to interactions with longitudinal thermal phonons. There are then three independent values of the third order elastic constants: these may be taken to be C_{111} , C_{112} , C_{123} . 1, 2, 3 are a mutually perpendicular set of axes and we take 1 as the acoustic wave propagation and polarization direction.

The attenuation per cm is

$$\Gamma = \frac{\pi^2 \hbar \omega}{60 \rho^3 v^{10} \beta^5} \left(\frac{kT}{h} \right)^4 \left\{ \omega T \int_{-1}^{+1} \frac{[G(x)]^2 dx}{1 + [\omega T(1 - \beta x)]^2} \right\} \quad (1)$$

where: v is the acoustic wave velocity; $x = \cos \theta$, where θ is the angle between acoustic and thermal phonon propagation directions. The rest of the notation is that of Simons. In our formulation

$$G(x) = A_{111} x^2 + A_{112} (1 - x^2) \quad (2)$$

where: $A_{111} = 3C_{11} + C_{111}$, $A_{112} = C_{12} + C_{112}$. In the temperature range for which $\omega T > 1$, the bracketed factor in Eq. (1) may be written as a finite series in powers of $(1/\omega T)$. The leading term is

$$A_{111}^2 [\tan^{-1}(1+\beta)\omega T - \tan^{-1}(1-\beta)\omega T].$$

This is the only term obtained in the previous formulations and it should be noted that it is proportional to A_{111}^2 only, rather than an average of several A_{ijk} . (This will be true in anisotropic crystals also; however, A_{112} will then be replaced by a combination of several A_{ijk} .) This term gives rise to the temperature dependences mentioned above, T^4 in the region $(1+\beta)\omega T \gg 1 \gg (1-\beta)\omega T$, and T^n ($n > 4$) in the region $(1-\beta)\omega T \gg 1$. The second term in the series is proportional to $(1/\omega T)$ and thus produces a T^n ($n > 4$) dependence even in the aforementioned higher temperature region. Taking $(1-\beta)\omega T \ll 1 \ll \omega T$, we find for the second term,

$$1/\omega T [8/3(A_{111} - A_{112})^2 + 4A_{111}(A_{111} - A_{112})(1 - \log 2\omega T)]$$

If the third order elastic anisotropy is large, so that $A_{111}^2 \ll A_{112}^2$, then the second term will be of equal or greater importance than the first in some range of ωT and the resulting temperature dependence will depart from T^4 .

The occurrence of large anisotropy may not be unusual.

We note that for quartz, taking the 1 axis in the x direction,

$$A_{111} = +0.459 \times 10^{12} \text{ dynes/cm}^2, \text{ while } A_{112} = -3.38 \times 10^{12}$$

dynes/cm². The second term is then equal to or larger than the first for $\omega\tau \lesssim 40$. For $\omega/2\pi \approx 10$ Gc/sec and using values of τ calculated by Maris, we therefore expect $n > 4$ in the temperature range $20^\circ\text{K} \lesssim T < 40^\circ\text{K}$, the upper limit being set by $\omega\tau > 1$. Jacobsen's measurements of longitudinal wave attenuation on the x-axis of quartz at 9.4 Gc/sec and 24 Gc/sec exhibit an $n \sim 6$ dependence in this temperature range.

Pomerantz has compared the absolute value of longitudinal wave attenuation with the earlier theory (first term only) using values of A_{111}^2 measured by the collinear parametric interaction technique. In those cases for which A_{111}^2 is unusually small the measured attenuation was greater than the predicted value. This result is expected on the basis of our formulation.

Finally, we note that for transverse waves propagating on even-fold axes the strictly collinear interaction is forbidden by symmetry. That is, the third order elastic constant for these processes (A_{666} or A_{555}) vanishes identically. However, the term in $1/\omega\tau$ may still be present and must then be compared with the Landau-Rumer attenuation.

B. 3) Temperature Dependence of Microwave Phonon Attenuation

There has been relatively little systematic measurement of the attenuation of microwave phonons. Such measurements are desirable in order to check the theories outlined above, and also to perhaps suggest empirical correlations of the properties of various crystals with the microwave phonon attenuation. We have therefore measured the attenuation of longitudinal and transverse 9 GHz phonons propagating along various axes of a variety of crystals. The work is described in detail in Quarterly Reports 2, 3, 4 and 9.

In general, the results may be summarized as follows: there appear to be two classes of materials, the "simple" and the "complex". The "simple" crystals are elements, e. g., Ge and Si, or cubic compounds containing few atoms per unit cell, e. g. MgO, GaAs. The "complex" crystals are those with many atoms per unit cell, e. g., garnets, rutile. Broadly speaking, the simple crystals have a rapid temperature dependence of attenuation, i. e., $\alpha \sim T^n$ where $n \approx 4$. The rapid increase of attenuation with increasing temperature means that these materials have good transmission properties only at low temperatures. The complex crystals, on the other hand, tend to have rapid increase of attenuation at low temperatures, but at higher temperatures

the attenuation varies as T^n where $n < 1$; phonon echoes can be seen at room temperature in these materials. We describe these results in greater detail below.

"Simple" crystals: Typical results of measurements of the temperature dependence of the attenuation of 9 Gc/sec phonons are shown in Fig. 1. Measurements have been made on crystals of quartz, CdS, GaAs, Ge, Si, CaF_2 , Al_2O_3 and MgO in several directions and modes of polarization. The attenuation in most of the materials is proportional to T^n , where the average value of $n = 4.1 \pm 1.2$ for the fast transverse waves, 4.0 ± 1.7 for the slow transverse waves, 4.8 ± 1.4 for the longitudinal waves. For MgO and Al_2O_3 the attenuation is proportional to the frequency of the sound between 3 and 9 Gc/sec. An empirical correlation of the data is that the attenuation of 9 Gc/sec phonons is 3 dB/cm when $(T/\Theta) \approx 0.1$, where Θ = Debye temperature of the crystal. Values of the third order elastic constants were used to make absolute comparisons of the theory of attenuation by three-phonon processes with the data. The agreement is good in some cases but not in others.

"Complex" crystals: "Complex" crystals, i. e., those that contain many atoms per unit cell, seem to have temperature dependences of attenuation that are not single powers of the

temperature over the entire temperature range from He to room temperature. An experimental curve for YAlG is shown in Fig. 2. The attenuation increases $\propto T^2$ between $T \geq 40^\circ\text{K}$ to $T \leq 100^\circ\text{K}$; it increases more slowly, $\propto T^1$, between $T \geq 100^\circ\text{K}$ and $T \leq 320^\circ\text{K}$. This kind of behavior has been measured by us in rutile (TiO_2), YIG, and YGaIG. The curve for Al_2O_3 , included among the simple crystals, shows a tendency toward complex behavior. The obvious advantage of these materials is that the attenuation at room temperature is low enough to permit observation of phonon echoes.

The theoretical explanation of the difference between simple and complex crystals is not clear at present. According to the theory described in Sec. IA, the attenuation depends upon the magnitude of $\omega\tau$, where ω = circular frequency of the ultrasound and τ = lifetime of the thermal phonon with which the ultrasound interacts. For $\omega\tau > 1$, i. e. at low temperatures where τ is large, the attenuation is $\propto \omega\tau^4$. At high temperatures where τ is short such that $\omega\tau \ll 1$, $\alpha(T)$ depends upon the temperature dependence of τ . In general, the attenuation is lower if $\omega\tau \ll 1$ than it would be if $\omega\tau \gg 1$. Thus one expects that as the temperature increases the attenuation will cease to increase at a high power of T . It seems that the criterion for good ultrasonic

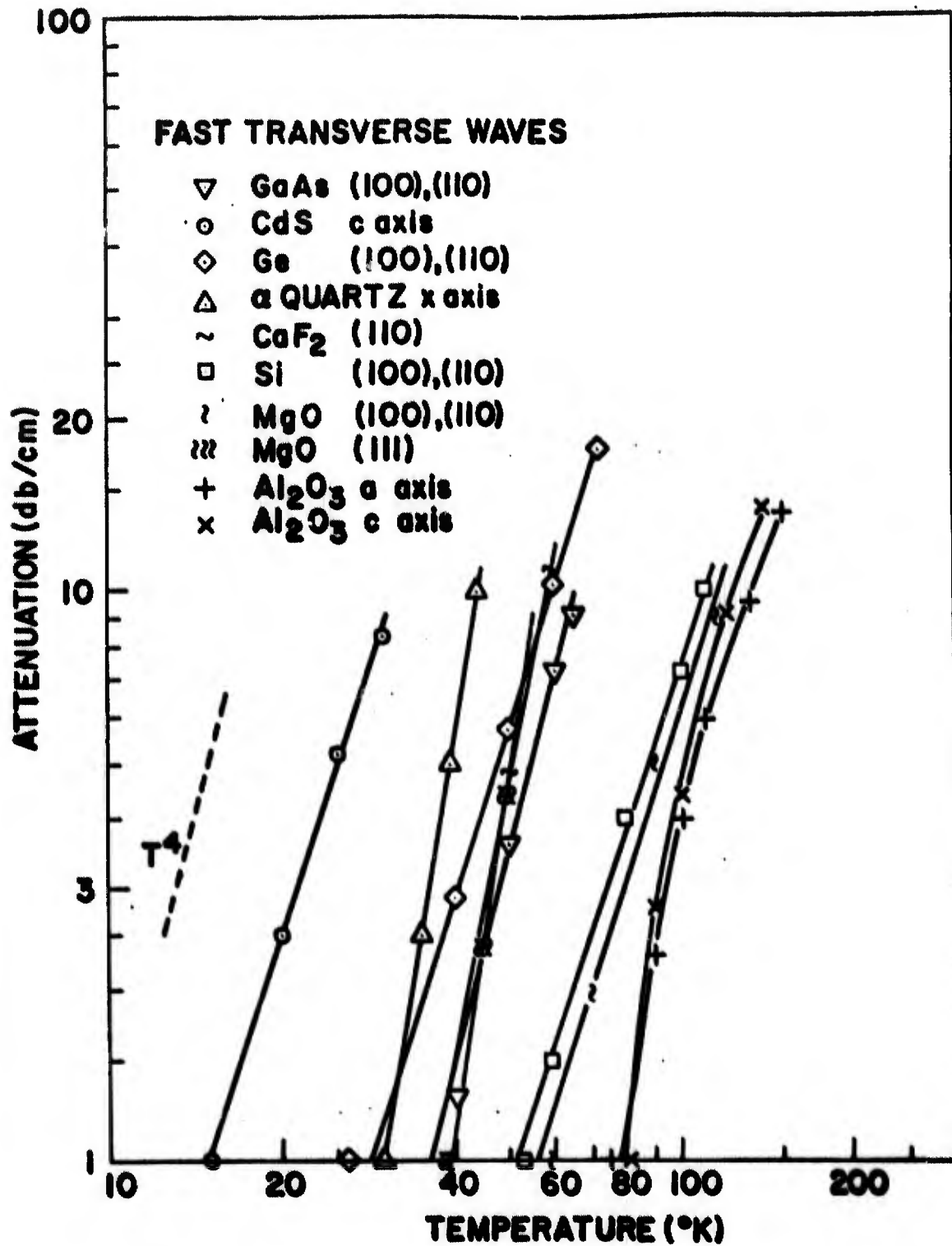


Figure 1 Attenuation of fast transverse 9 Gc/s phonons vs. temperature.

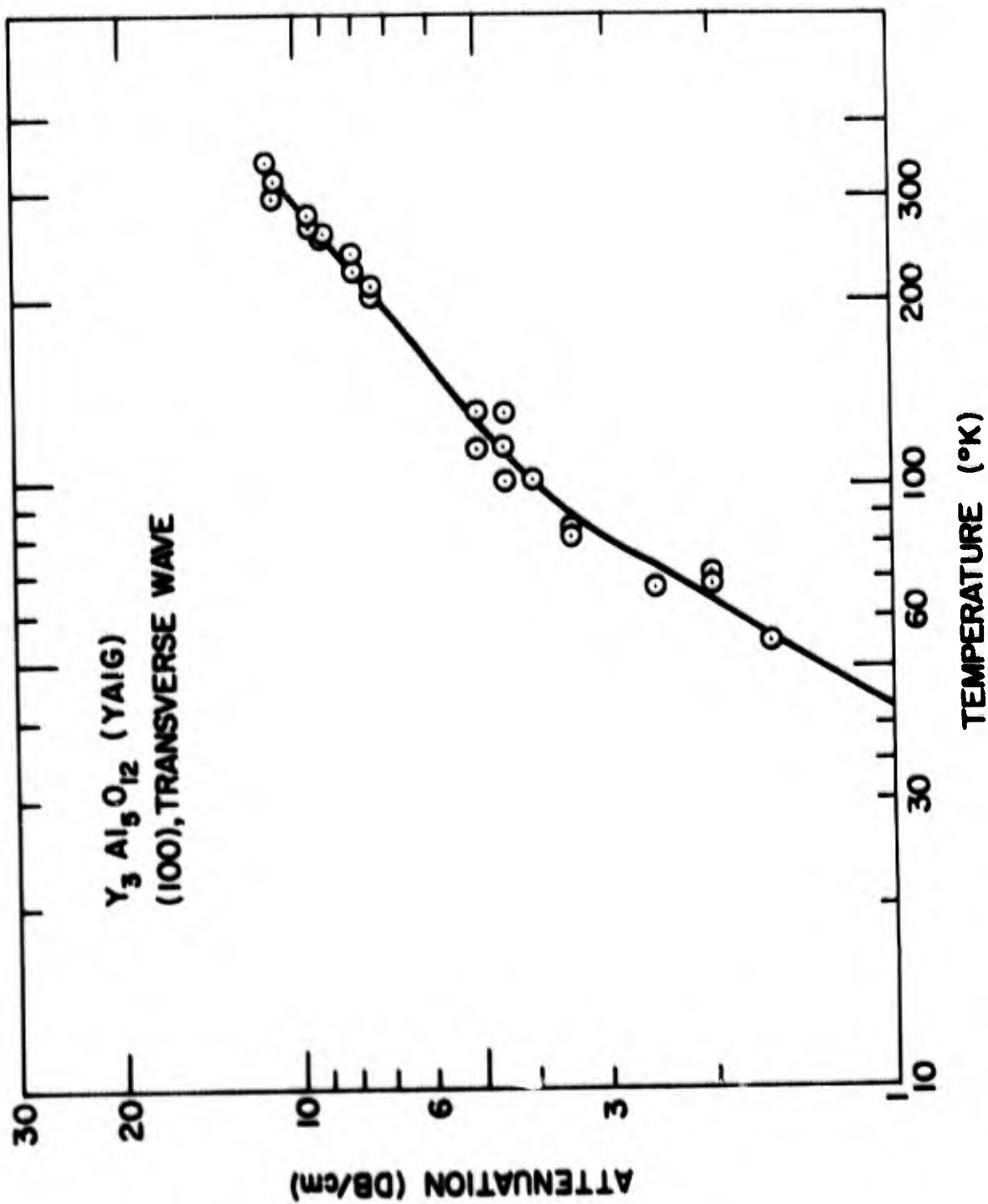


Figure 2 Temperature dependence of attenuation in Yttrium Aluminum Garnet. The frequency of the wave is 9 GHz and it is polarized transverse to the direction of propagation which is the (100) axis.

transmission is that T should be small ($\omega T \ll 1$) at as low a temperature as possible. There remains the theoretical problem of explaining why T becomes smaller at lower temperatures for complex crystals than it does for simple crystals.

B. 4) Attenuation of Higher-than-Thermal-Frequency Ultrasound

The properties of very high energy transverse acoustic phonons ($h\omega \gg k_B T$) have been studied. Such phonons have been produced in non-radiative transitions in paramagnetic salts. The role of four-phonon processes in the decay of such high energy phonons from the lowest (transverse) branch was discussed. The effects of the quartic anharmonic interaction, as well as the cubic anharmonic interaction calculated in the second Born approximation, were included. The largest four-phonon processes were found to be $t+t \leftrightarrow t+t$ and $t+l \leftrightarrow t+t$. A comparison of the four-phonon decay rate with the three-phonon decay calculated by Orbach and Vredevoe showed that both processes are very small at low temperatures, whereas at intermediate temperatures the three- and four-phonon decay rates are comparable in magnitude, the four-phonon rate being proportional to $\omega^2 T^5$ in the high frequency region, i. e. for $h\omega \gg k_B T$. The relation between the high energy attenuation and previous

results obtained for low energy ($hw \ll k_B T$) was discussed.

See Quarterly Report No. 10 for details of this work.

C. Heat Pulses in Quartz and Sapphire

Experiments were performed on the propagation of heat pulses in single crystal dielectric materials at temperatures sufficiently low that only boundary and "defect" scattering should be effective in deflecting the phonons from direct rectilinear flow. Such heat pulse experiments can give more direct and unambiguous information than the usual thermal conductivity measurements on how the thermal phonons travel across the crystal since their trajectories can be resolved both in time and in space. The technique is somewhat similar to pulse measurements of the attenuation of microwave phonons except that the phonons have a much higher frequency, are incoherent, and are not monochromatic. Also, the thermal detector is sensitive to the arrival of scattered phonons arriving at various times.

Both X-cut and Z-cut samples of natural quartz and synthetic sapphire obtained from the Valpey Crystal Co. were investigated. They were cylindrical in shape ($D = 5/8$ in.) with polished end faces on which were evaporated thin metallic films to generate and detect the heat pulses. The detector was a thin alloyed

superconducting film of thickness $\sim 1500 \text{ \AA}$, whose resistance was sensitive to temperature changes. A 6% Sn-94% In alloy was used at 3.8°K and a 35% Bi-65% Pb alloy at 8.5°K . Because of the circular shape of the detector, the important phonons were those whose net motion lay near a cone centered on the axis of the sample, the cone angle (θ) being determined by the length (L) and diameter (d), where $\tan \theta = d/2L$. The major findings for quartz and sapphire for the temperature range 3.8 - 8.5°K were that (1) approximately $1/15$ of the heat flux for quartz and $\sim 1/4$ for sapphire reached the detector in essentially uninterrupted direct rectilinear line-of-sight propagation ; (2) the remainder of the heat flux was scattered, the angular and temperature dependencies being those characteristic of a small-angle scattering process ; (3) the velocities of the unscattered heat pulses are not given by the conventional longitudinal and transverse sound velocities, but by suitably defined "wave" (energy) velocities ; (4) related to this, more than two unscattered transverse heat pulses were observed in quartz. This is discussed in detail in Quarterly Progress Report No. 4.

The work on heat pulses in sapphire as a function of temperature provided a number of interesting and somewhat unexpected results. One major purpose of the experiment was to try to

observe the propagation of heat in the "second sound" mode, which has a velocity \approx velocity of sound/ $\sqrt{3}$. The observed onset time of the arriving heat pulses for the longitudinal phonons is essentially constant for the temperature range 4-40°K and the onset time for arrival the transverse phonons is almost constant, increasing by only ~ 5% over this temperature range. As the temperature increases the amplitude of the sharp transverse pulse relative to the longitudinal pulse decreases; also by 18°K appreciable phonon-phonon scattering is present which gives rise to an additional diffuse maximum at times substantially later than either the acoustic energy transport time or that expected for second sound. From 40°K-54°K, no observable heat arrives at the acoustic velocity, but the heat arrives instead by diffusion at a very much later time in agreement with thermal conductivity results. Near 4°K a phonon echo is observed at three times the transit time at the transverse velocity. It appears that second sound does not exist in sapphire. A detailed discussion of this work is given elsewhere in this report.

D. Thermal Relaxation Times of Metal Films on Insulating Substrates

The thermal decay times of thin pure indium, In-Sn and

Pb-Bi films on quartz and sapphire substrates were measured. Thermal decay times of the alloy films were measured near their superconducting transitions, i. e., $T \sim 3.8^{\circ}\text{K}$ for In-Sn and $T \sim 8.5^{\circ}\text{K}$ for Pb-Bi; for the pure indium film measurements were made in the range $4\text{-}300^{\circ}\text{K}$. These times were compared with the predictions of two models for the heat loss process at low temperatures. The first assumes perfect thermal contact between the two materials and corresponds to perfect black-body phonon radiation from the film into the insulator. The second, which predicts up to 40% lower rate of heat loss, corresponds to an acoustic mismatch model in which the reflection of phonons at the interface is considered. Experimentally, it was found that the results for the indium and indium-tin films approached the predictions for the perfect thermal-contact model, while the results for the lead films showed a slower rate of heat loss than either model predicts.

At higher temperatures, the pure indium films were found to thermally relax in qualitative agreement with the thermal diffusion theory of heat transport, although there were some quantitative discrepancies. The initial part of the thermal decay of a 2200 \AA film on a sapphire substrate was measured to be as fast as $\sim 2 \times 10^{-9}$ sec near 100°K , increasing to about

8×10^{-9} sec at room temperature. The decay times were found to be longest (up to $\sim 30 \times 10^{-9}$ sec) below 10°K , where the heat transport is predominantly by ballistic phonon flow. The decay times for a 2700 \AA film on a quartz substrate were found to lie between 13 to 30×10^{-9} sec in the range of temperatures from 4° to 300°K . This work is described in detail in Quarterly Progress Reports 10 and 11.

E. Lattice Dynamical Theory of Displacive Ferroelectrics and Antiferroelectrics

Displacive ferroelectricity and anti-ferroelectricity are manifestations of anharmonic phonon interactions because in a displacive ferro- (or antiferro) electric the harmonic restoring force for an optical mode vanishes, and it is the anharmonic force that stabilizes the structure (in the ferroelectric phase).

Ferroelectricity: The purpose of our theoretical study was to make a detailed derivation of the free energy function from a microscopic Hamiltonian describing the lattice dynamics of the anharmonic crystal. One obtains in the linear anharmonic approximation a free energy F which is a power series in a set of microscopic order parameters. The set of microscopic order parameters consist of (a) the thermal expectation values of the normal coordinates of all the optical branches in the long

wavelength limit which determine the change of the equilibrium ionic positions in the ferroelectric transition and (b) the thermal expectation values of the normal coordinates of the acoustic branch in the long wavelength limit which determines the strain tensor. This is a more general free energy power series than the phenomenological free energy introduced by Devonshire because the latter is expressed in terms of a smaller set of order parameters, e. g. the entire set of optical branch order parameters is replaced by the polarization per unit volume. However it is shown that when the frequency of the soft optical branch (in the long wavelength limit) is much smaller than the frequencies of the other optical branches the general free energy function reduces to the Devonshire form. The coefficients of the free energy function are then explicitly evaluated in terms of anharmonic coupling parameters. A complete discussion of this work is given in Quarterly Progress Report No. 11.

Antiferroelectricity: The phenomenological theory of antiferroelectrics studied by Kittel and Cross describes the antiferroelectric by a free energy power series in the polarization of two sub-lattices. The two sub-lattice theory cannot in general give a complete description of the atomic displacement in the antiferroelectric transition because the polarization represents

only a weighted average of the displacements. We have studied a microscopic theory based on lattice dynamics which inherently gives a complete description of the atomic displacements in the antiferroelectric transition. A free energy power series in a complete set of atomic displacements compatible with the translation symmetry of the antiferroelectric phase has been constructed and the nature of the possible antiferroelectric solutions corresponding to minima of the free energy has been examined. The main conclusions of the theory are (a) the wave-vectors of the normal coordinate displacements compatible with the translational symmetry of the antiferroelectric phase form a finite group and all extrema of the free energy form subgroups of it. (b) There will in general be a net polarization in the antiferroelectric phase, except for a few very special cases.

A more detailed preliminary report of this work is included in Quarterly Progress Report No. 12. This preliminary version contains several errors which will be corrected in a future publication.

II. Phonon Interaction with Paramagnetic Ions

The interaction of microwave phonons with paramagnetic ions can be studied in order to obtain interesting effects on phonons traveling through a resonant medium, or to better understand the relaxation of the excited spin states to the lattice. In the former category we discuss experiments on: (A) the signal velocity of the phonons when the spins are in a state of negative temperature (inverted population), and (B) the transient operation of high gain phonon masers. In the second category are experiments on (C) spin-lattice relaxation by phonon avalanche, and observation of phonons emitted during avalanche relaxation.

A. Signal Velocity in a Region of Resonant Emission

Measurements of the velocity of propagation of ultrasonic pulses propagating through a maser amplifier were conducted. Previously reported measurements and theory showed that the signal velocity decreases in the neighborhood of a resonance absorption line. In the case of emission, theory also predicts a decrease in velocity. The experimental results, however, do not agree with that conclusion: no velocity change from the "off resonance" value was observed.

A phonon maser utilizing the $\text{Ni}^{2+} \Delta M = 2$ spin-resonance

transition in MgO at 1.6°K was used in the experiments. 0.5 μsec ultrasonic pulses were generated in a quartz transducer bonded to the 1.5 cm MgO crystal. Population inversion was accomplished by adiabatic rapid passage through the $\Delta M = 1$ transitions at x-band.

The experimental results are illustrated in Fig. 1. Echo patterns are shown for 15 db amplification, for 15 db absorption, and for zero interaction (i. e., off resonance). For the amplification condition the input was 15 db smaller than for the other two conditions in order to avoid saturation of the resonance. If the power is high and saturation is allowed to occur, the amplified signal exhibits the well known pulse-sharpening effect. In Fig. 1 the velocity of the amplified pulse is seen to be unchanged from the off-resonance value. The attenuated pulse, however, exhibits the characteristic velocity decrease (in this case ~ 15%),

$$\Delta(1/v) \approx \beta(\omega)/\delta. \quad (1)$$

$\beta(\omega)$ is the absorption per cm at the input frequency, ω , due to the resonance transition centered at ω_0 . δ is the half-width at half-amplitude due to either homogeneous broadening ($1/T_2$) or small (spatial) scale inhomogeneous broadening.

This work is described in detail in Quarterly Progress Reports 1 and 3.

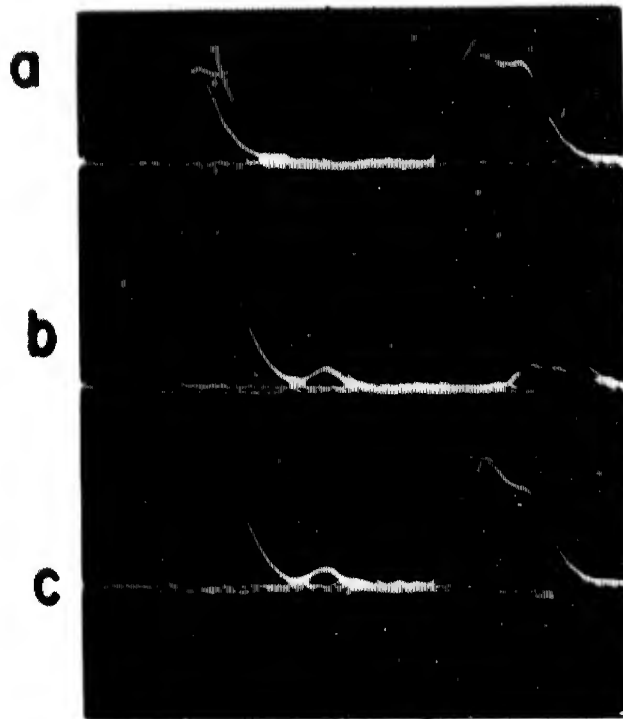


Figure 1 Oscilloscope traces showing effect of Ni^{2+} resonance interaction on ultrasonic signal velocity. Time runs from left to right. The first pulse is a bond echo and has traveled through the quartz transducer only. The second pulse has made one round trip through the MgO . The time between pulses is $2.27 \mu\text{sec}$. (a) 15-db amplification, ultrasonic frequency on peak of $\text{Ni}^{2+} \Delta M = 2$ resonance, (b) 15-db attenuation, on resonance, input power 15 db higher than in (a). (c) Off resonance, input power same as (b).

B. Transiently Operated Acoustic Masers

Maser amplification at both x-band and Ku-band (see section on signal velocity) frequencies was achieved in Ni^{2+} and Fe^{2+} doped MgO crystals. Several different modes of operation were investigated. More recently, this work has led to the observation of avalanche relaxation in a phonon bottlenecked lattice, and to the observation of the phonons generated in the avalanche.

In the course of the investigation of 9 Gc/sec ultrasonic amplification following adiabatic rapid passage through the $\Delta M = 1$ spin resonance transitions of Ni^{2+} and Fe^{2+} in MgO, we observed, under certain conditions described below, large gains (-28 dB in Fe^{2+} doped crystals) at 1.6°K due to stimulated emission in phonon-photon double quantum transitions between the $S_z = \pm 1$ levels. Two-photon stimulated emission has been previously proposed as a LASER mechanism and phonon-photon double quantum absorption was reported earlier. In nearly equally spaced level systems the phonon-photon transition is especially favorable compared with the photon-photon case. This may be seen from the standard perturbation theory expression for the double quantum matrix element by noting that for exactly equal level spacings the two terms (which correspond to different orderings of the perturbations) cancel if both perturbations are

dipolar, but add if one is dipolar and the other is quadrupolar.

The experimental configuration is shown in Fig. 2. Longitudinal ultrasonic waves were generated by the usual method involving a tunable (8.5 Gc/sec - 9.7 Gc/sec) re-entrant cavity and a quartz transducer. The 3 mm diameter quartz bar is bonded to a doped MgO crystal which lies along the axis of a silver coated ceramic cavity operating in the TE_{011} mode at ~ 9 Gc/sec. The microwave magnetic field, H_1 , required for passage is provided by this cavity. Both cavities are driven from magnetrons, and H_1 fields ~ 50 Oe are attainable. A sweep field > 300 Oe is provided by coils wound axially on the ceramic cavity and driven by a thyatron pulser. The optimum angle of the external magnetic field H_0 with respect to the crystal-cavity axis is 45° , in order to have a component of H_1 perpendicular to H_0 and a component of the sweep parallel to H_0 . However, this is also the angle for maximum spin-phonon interaction with the $\Delta M = 1$ transitions.

The ultrasonic pulse is timed to enter the MgO immediately after the sweep ends. For ordinary MASER operation the H_1 pulse is also terminated at that time. For the double quantum process, however, the H_1 pulse is left on, following the sweep, for one round trip of the ultrasonics through the MgO as shown

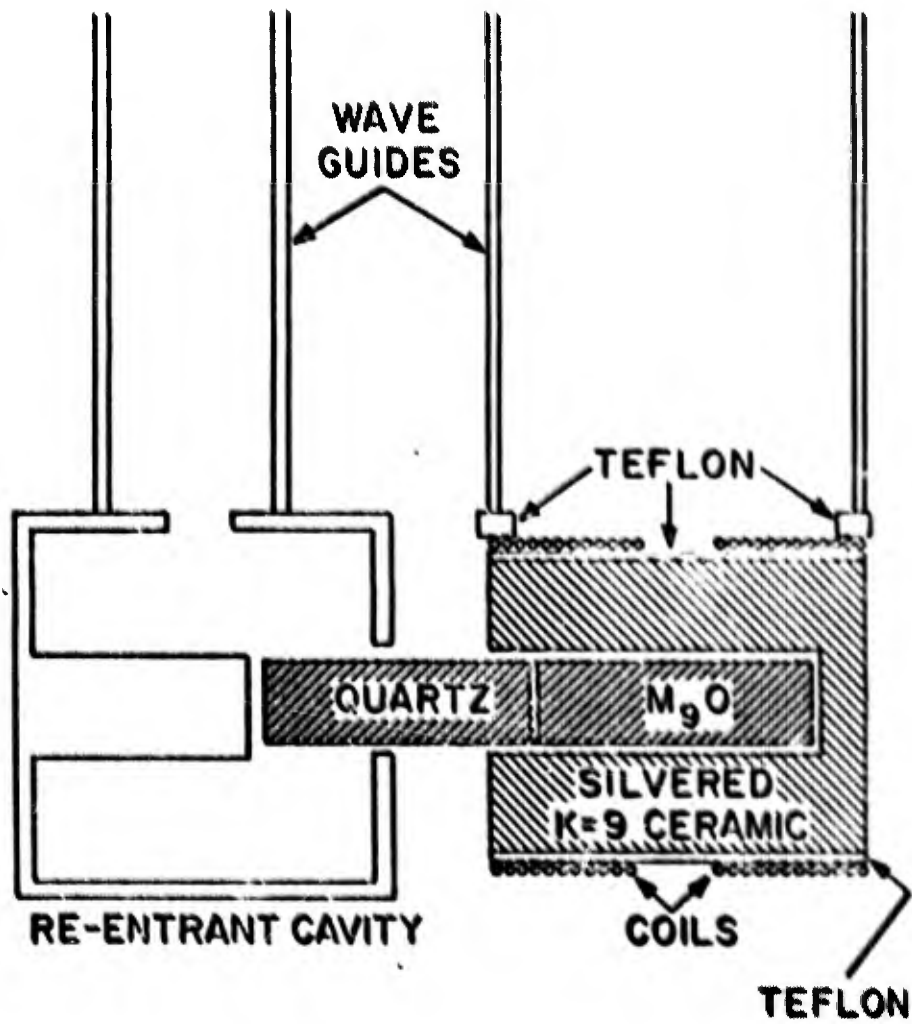


Figure 2 Schematic diagram showing cavity and crystal arrangement.

in Fig. 3. In the presence of the strong H_1 field the ultrasonic pulse then stimulates double quantum emission in the inverted $\Delta M = 2$ transition. The propagation time is $2.2 \mu\text{sec}$ in the crystals used, the sweep time is $\sim 2 \mu\text{sec}$ and, therefore, a $5 \mu\text{sec}$ H_1 pulse is used. An observed echo pattern in iron doped material is shown in Fig. 5.

When H_1 is very large the usual perturbation treatment of double quantum transitions is not adequate. By performing the calculation in the coordinate system rotating at angular velocity ω the effect of H_1 is treated exactly. H_0 is then also transformed to the rotating frame and introduced as a perturbation. The double quantum resonance then appears as though it were a first order $\Delta M = 2$ transition at frequency $|\Omega - \omega|$. This is similar to the treatment of rotary saturation or double irradiation resonance in $S = 1/2$ systems. The transformation is illustrated schematically in Fig. 4.

The calculated double quantum matrix element is

$$M = \frac{1}{4} \frac{H_1}{H_e} \left(1 \pm \frac{H_0^*}{H_e} \right) G_e$$

where the \pm sign is taken according as $\Omega < \omega$: $H_0^* = (H_0 - \omega/\gamma)$, and $H_e = (H_0^2 + H_1^2)^{1/2}$. Unlike the perturbation expression, M

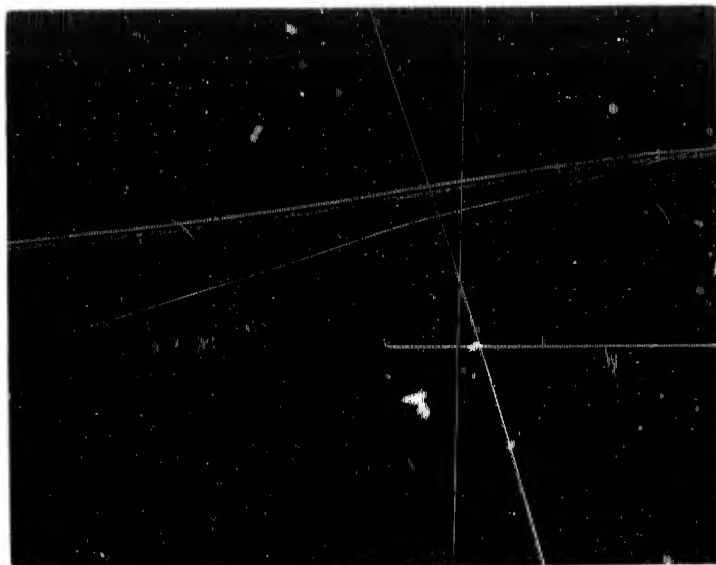


Figure 3 Sweep field and microwave pulses, showing relative timing for inversion and double quantum amplification.

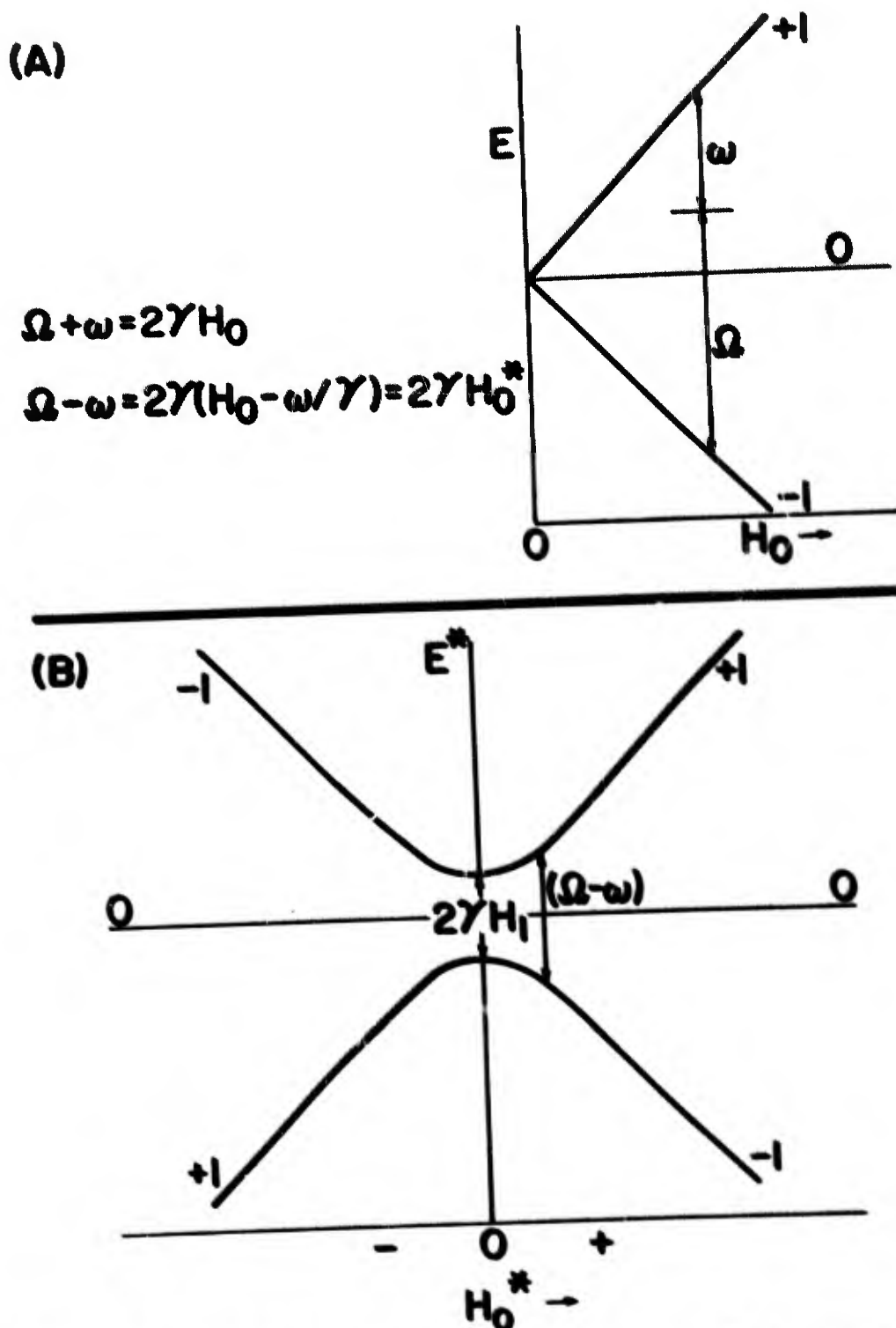


Figure 4 Energy level diagrams for $D = 0$. A typical double quantum transition is shown. A. In the laboratory system. B. In the rotating system. The various levels are labeled according to their spin quantum numbers for large H_0^* .

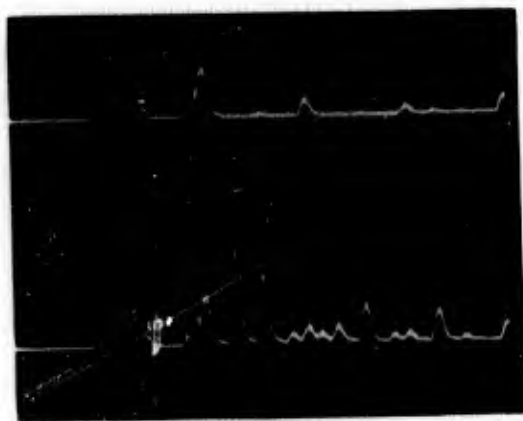


Figure 5 Oscilloscope traces showing amplification in Fe^{2+} (upper trace), and off resonance echo pattern (lower trace). Pulses having the same amplitude in both traces are bond echoes. Only the first MgO echo has experienced amplification over its whole propagation path.

does not diverge for large H_1 . The maximum value of M occurs for $H_1/H_e = \sqrt{3}/2$ and is equal to $(3\sqrt{3}/16) Ge$. This may be compared with the single quantum $\Delta M = 2$ transition for which $H_U = GeS_x^2 \cos \Omega t$ and the matrix element is $1/4 Ge$. For the same Ge the double quantum interaction is larger than the single quantum.

Details of this work are in Quarterly Progress Reports 1, 3, 5, 6, 7.

C. Avalanche Spin Lattice Relaxation

It was noted in the experiments on maser amplification that in the case of Fe^{2+} the observed ultrasonic gains were considerably smaller than predicted theoretically from the known absorption magnitudes. A possible explanation for this behavior was that the spins were relaxing so rapidly that the ultrasonic pulse did not see a fully inverted population over its whole propagation path.

This type of relaxation is expected to occur for spin systems which are so strongly coupled to the lattice that the rate of spontaneous phonon emission exceeds the rate at which the phonons decay to other modes or escape from the crystal. Under such conditions the phonon population builds up rapidly by amplified

spontaneous emission. The inverted spin population drops suddenly to zero and a phonon avalanche is formed.

Experimental measurements on the Ni^{2+} system showed the presence of avalanche relaxation occurring in about 20 microseconds after inversion. The Fe^{2+} system, which is more strongly coupled to the lattice decayed so fast (estimated to be $\sim 10^{-7}$ seconds) that measurements could not be made on the spin system. However, because of this fast decay a large phonon flux occurs in the avalanche and these phonons were detected at one end of an MgO rod in which the spins on the opposite end had been inverted. These results are reported in detail elsewhere within this Final Report.

III. Phonon Interaction with Static Defects

Phonons can be scattered by static defects in the lattice, such as dislocations, and dissolved impurities. The scattering mechanism may be of the mass-defect type. This is observed in heat pulse transmission in untreated alkali halides. Another scattering process, arising from the relaxation of electrons bound to donors in semiconductors will also be discussed below.

A. Heat Pulses in Alkali Halides at Low Temperatures

Further studies of the propagation of heat pulses, similar to those previously reported for quartz and sapphire, were made on several alkali halides. These included NaCl, KCl, KBr, and KI. The objective was to determine the nature of the heat-pulse propagation in high-purity crystals at temperatures near that at which the thermal conductivity is a maximum. It is at such temperatures that observation of "second sound" in insulating crystalline media, if it occurs, is most likely to be observed. Since superconducting film thermal detectors are used, this temperature must be compatible with the operating temperature of the detector used (approx. 8.0°K). This condition is approximately met by several of the alkali halides. For these experiments, the heat pulses observed for the best NaCl and KCl

crystals were qualitatively similar to those observed for quartz, since they showed some sharp structure superposed on a broad scattered background. The heat pulses observed for the KBr and KI crystals, on the other hand, showed only the broadened, scattered type of response, presumably because of some type of defect scattering.

The type of heat pulses observed in NaCl depended strongly on the sample preparation. The effects were very similar to those observed in measurements of the thermal conductivity. The thermal conductivity was approximately two orders of magnitude larger for chlorine-treated crystals grown from reagent-grade material than for single crystals obtained from Harshaw. This was presumably due to the effects of treating NaCl with chlorine in reducing the OH radical impurity (or the oxygen band). The chlorine-treated crystal exhibited sharp heat pulses arriving at times corresponding to the velocities for the various polarizations of the acoustic vibrations. However only a rather small fraction of the total energy flow is apparently by uninterrupted, rectilinear, phonon propagation; the remainder of the phonons are scattered by some defect mechanism. The reagent grade Harshaw crystal exhibited mainly diffusive heat flow.

The velocities of the pulses were in better agreement with the wave (energy) velocities, rather than with the phase velocities, as had previously also been found for quartz. These wave velocities were estimated by calculating the phase velocities from the elastic constants extrapolated to 0°K . The wave velocities were then roughly estimated by a graphical method from the phase velocities for the special azimuthal angles $\phi = 0^{\circ}$ and 45° , for which these phase velocities are stationary with respect to ϕ .

The pulse shape was also examined at 8.0°K . Although the pulses were broader, this could have been caused by the slower detector. In any event, the discrete pulses, arriving at the acoustic velocity, were still present and, thus, a considerable fraction of the phonons even at this elevated temperature do not have their flow effectively interrupted. A significant number of phonons must have collided only with large scale defects (since such scattering is relatively independent of frequency and hence of temperature) or have suffered only collinear or near collinear phonon-phonon normal process collisions (since these would not appreciably change the velocity of the energy flow). The phonons within the sharp pulses do not show any shifts in velocity at all comparable to those pre-

dicted for second sound. The scattered background phonons, of which there is a large majority, also did not show any particular changes as the temperature is raised from 3.8 to 8.0°K.

The results for zone-refined KCl were rather similar to those for NaCl, with the background scattering being somewhat greater (Fig. 2c) relative to the sharp pulses. Only traces of the sharp pulses were present in Harshaw KCl. Thus, the defect scattering appeared to be somewhat larger for the best KCl used than for the best NaCl, even though the chemical purity of the zone-refined KCl is undoubtedly much greater. Calculations of the energy velocities from the known elastic constants again gave better agreement with the observed heat-pulse velocities than did the phase velocities.

Crystals of KI obtained from Harshaw and of KBr treated with bromine gas were also investigated at 3.8°K. For both of these crystals, the scattering was so great that the thermal flow was principally a diffusive one, with no discernible sharp structure present. Details of this work are given in the Fifth Quarterly Progress Report.

B. Phonon Interaction with Shallow Impurities in Ge and Si

Measurements of the attenuation of 9 GHz microwave phonons in n-type Ge and Si have revealed strong interaction of these phonons with the donors. A theory of this interaction involving relaxation of electrons among the donor energy levels under the influence of the phonon strain agrees well with the experiments. This new mechanism of attenuation may also be important in determining thermal phonon mean free paths as observed in thermal conductivity and thermoelectricity.

The experiments were measurements of the attenuation of 9 GHz ultrasound as a function of temperature. The attenuation of the pure modes along the (100) and (110) axes was observed in Ge samples doped with Sb, P, Bi, and As in concentrations between 10^{13} /cc and 10^{16} /cc, and in Si doped with P to about 5×10^{16} /cc. Experimental results for the shear wave propagating in the (100) direction of Ge doped with about 3×10^{15} /cc of various donors are given in Fig. 1. The dashed curve is an earlier measurement of the attenuation in pure Ge. The excess attenuations above the dotted curve are attributed to the donors. Some notable features of these observations are:

- 1) The temperature dependences of the attenuation are different,

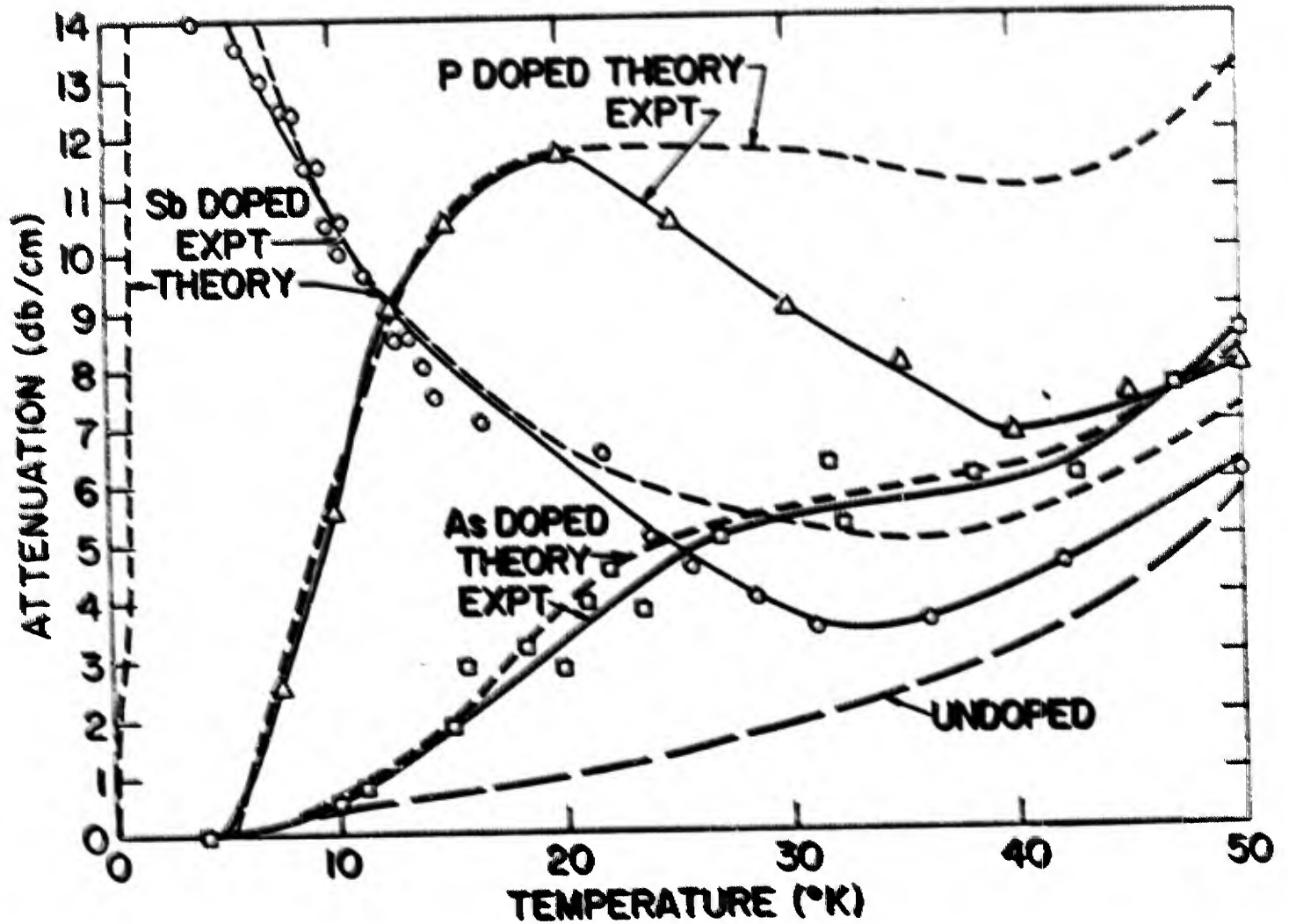


Figure 1 Attenuation of 9 GHz shear waves propagating along (100) direction in Ge. The impurity concentration of each donor is $\approx 3 \times 10^{15}/\text{cc}$.

depending upon the chemical species of the impurity. 2) The largest excess attenuations are for ultrasonic modes whose elastic constants depend on c_{44} . (By the elastic constant, c , of a mode we mean that $c = \rho v^2$ where ρ = density and v = velocity of that mode.) 3) The excess attenuation increases in proportion to the impurity concentration, and is quite large (of order 10 db/cm) for such low concentrations of impurities (less than a part per million). 4) The attenuation is due to neutral impurities, since at these low temperatures and concentrations the donor electrons are trapped in localized impurity states. The experimental result for P doped Si has the significant difference that the mode that suffers excess attenuation is the shear wave whose elastic constant is $(C_{11} - C_{12})/2$; the other shear mode, whose elastic constant is C_{44} , is unaffected by the impurities. The dependence on the mode of polarization indicates that the many-valley structures of the conduction bands of Ge and Si are involved in the attenuation processes. Particular shear strains can lift the degeneracy of the conduction band minima; it is only these shear waves that are attenuated by the impurities.

The mechanism we propose to explain these measurements is that the ultrasonic strain induces electronic relaxa-

tion among the energy levels of the donors. Relaxation attenuation results when the elastic energy of a body does not respond instantaneously to stresses applied to it. A calculation of the relaxation attenuation due to the donors gives:

$$\alpha = \frac{2N_3(T)\Xi_u^2}{3cvkT} \frac{\omega^2 T}{1 + \omega^2 T^2} \quad (1)$$

where α = attenuation in nepers/cm, $N_3(T)$ is the density of electrons in the triplet state of the donor, Ξ_u = shear deformation potential constant of the band structure, c = elastic constant, v = sound velocity, ω = ultrasonic frequency $\times 2\pi$, T = relaxation time for electrons in the triplet state. The dotted curves in Fig. 1 are the theoretical predictions of Eq. (1), with the background attenuation of pure Ge added in. Constant values of T were chosen in order to fit the data at about 12°K. The theory gives good agreement with the experiments, except at temperatures $> 20^\circ\text{K}$. Our calculations of $N_3(T)$, however, have not included electronic excitation out of the ground states and therefore the calculated values of α will tend to be higher than the experimental ones.

A rough measurement of the frequency dependence of α indicates that the attenuation is increasing with frequency at 10 GHz. This suggests that the relaxation process may be an

important scattering mechanism for thermal phonons in the liquid He temperature range. (A thermal phonon with energy kT at $T = 4^{\circ}\text{K}$ has a frequency of about 100 GHz.) Indeed, we find that the thermal phonons mean free paths as measured by thermal conductivity and by the thermoelectric power can be explained in detail by the donor-relaxation theory.

We have also observed attenuation due to acceptors in Ge and Si. We are presently trying to relate these measurements to the anomalies in the phonon mean free paths in p-type Ge and Si that have been known for some years.

Experiments were also begun to observe the interaction of thermal phonons, in the form of heat pulses, with electrical-ly active impurities in Ge and Si. In relatively pure Ge and Si sharp pulses are found when the heat is produced by joule heating. In P doped Ge the pulses seem to be somewhat broadened, indicating some scattering by the donors at 3.0°K .

When the heat is produced by shining a pulsed laser on the sample surface, there are additional signals detected. There is a signal that arrives essentially simultaneously with the application of the light; this is probably some kind of recombination emission which can traverse the sample. There is also

a long tail on the phonon modes, which has a relaxation time of the order of tens of microseconds. This is presumably due to the emission of phonons by electrons during recombination processes. These experiments have not yet included all the impurities and ranges of temperatures of interest.

IV. Phonon Interactions with Free Electrons

The interaction of phonons with electrons arises from the potential set up by the phonon strain. This potential can arise either from the basic property of a solid that the potential depends on the dimensions of the lattice, or, in particular crystals, because of the piezoelectricity of the crystal. Our work has been mostly with interactions of the former kind, viz. deformation-potential coupled interaction, but some work has also been done with piezoelectrically coupled interactions in GaAs. The coupling of the electrons to the phonons can be observed by measuring effects on either the electrons or the phonons.

Phonons propagating through an electron gas tend to carry the electrons with them. This creates an electric current, known as the acoustoelectric current. We discuss below measurements of the acoustoelectric currents produced by microwave phonons in GaAs. Because the phonons give energy and momentum to the electrons the phonons will be attenuated. This is observed in the experiments on GaAs, and also in the propagation of heat pulses in Ga metal. If the electron drift velocity is increased beyond the velocity of sound, the phonons can be amplified, instead of being attenuated, by the interaction

with the electrons. The amplification of microwave phonons in Ge by this mechanism is described below. The energy absorbed by the electrons can cause a change in electrical resistance of the material. Experiments to observe microwave phonons by this effect are discussed.

A. Acoustoelectric Effect of Microwave Phonons in GaAs

The signals consist of a negative pulse as the wave train passes contacts in one direction followed by a positive pulse which results from the wave train passing the contacts in the opposite direction after reflection from the end of the bar. We refer to the sum of the measured magnitudes of the negative and positive current pulses as I_{pp} . This pair of electrical pulses is repeated (with diminishing amplitude) as the wave train is successively reflected from the ends of the bar. As many as three pairs of pulses have been observed. The spacing of the pulses is appropriate to the velocity of a $\langle 001 \rangle$ shear wave propagating in the $\langle 110 \rangle$ direction in GaAs.

The dependence of the amplitude of the first pair of pulses on microwave power (which should be proportional to the acoustic power in the GaAs) is shown in Fig. 1. Theory predicts a linear dependence of acoustoelectric current on acoustic power until $e\phi_0$ becomes a substantial fraction of kT . Assuming the crystal

does not disturb the electric field in the cavity, the maximum value of $e\phi_0/kT$ at 17°K was about 0.13, which would not give a significant deviation from linearity. In practice, the disturbance of the electric field and also the imperfect polishing of the crystal would result in a rather smaller value than 0.13.

The dependence of the amplitude of the pulses on illumination level is shown in Fig. 2. The results can be explained in terms of an increasing electron concentration with illumination causing a greater current for a given strain but a greater attenuation of the sound. Weinreich has given the relation between the acoustoelectric current density (i_{ae}) and the attenuation constant for the sound due to the electrons (α_n)

$$i_{ae}(x) = (\mu/v_s) \alpha_n Q(x), \quad (1)$$

where v_s is the sound velocity and Q is the acoustic power per unit area. Equation (1) shows that if the sound is significantly attenuated through the crystal i_{ae} is a function of x . However, in a region of crystal with no contacts the total current must be continuous and, in the absence of an applied field, it must correspond to some average value of i_{ae} . The electric field distribution required to maintain the current constant and the deviations from the equilibrium electron concentration (N_0)

that produce this field would cause n to be a function of x , but this effect would be negligible when $e\phi_0 \ll kT$.) Writing $Q(0)$ for the incident acoustic power, α_L as the attenuation constant due to the lattice, and $\alpha_n = \beta N_0$, Eq. (1) becomes

$$i_{ae}(x) = \frac{\mu\beta N_0}{v_s} Q(0) \exp[-(\beta N_0 + \alpha_L)x]. \quad (2)$$

By differentiating with respect to N_0 one finds that the electron concentration for maximum current at a distance x is given by

$$N_0 = (\beta x)^{1/2}. \quad (3)$$

x is about 0.8 cm for the first pair of pulses and effectively about 2.8 cm for the second pair. Therefore the light intensity (or N_0) for maximum current is higher for the first pair than for the second.

This calculation also indicates that the attenuation due to the electrons at the light intensity for maximum current in the first pair of pulses is about 4 dB/cm. This value can be compared with the value calculated from the measured current using the equation (1), which is about 0.17 dB/cm. The value of $Q(0) = 740$ watts/meter² was obtained by an approximate calculation and the mobility at 20° K was estimated to be 0.5 meters²/V sec. There is an order of magnitude discrepancy between these two determinations of α_n . This

may be due in part to an overestimate of Q_0 because of the uncertainty of the field configuration in the cavity with the sample in it and the loss of acoustic power due to scattering from material near the surface that was damaged by the cutting of the sample. It is expected that this discrepancy can be reduced by improved sample preparation. In view of the uncertainties in the values of $Q(0)$, μ and i_{ae} , we consider the agreement to be reasonable.

The temperature dependence of the peak to peak current of the first pair of pulses at constant illumination is shown in Figure 3. The interpretation of this curve is difficult at present owing to the uncertainty in the temperature variation of some of the parameters, but it can be given in general terms.

Region 1 (below 15°K). In this temperature range, the concentration and mobility of the electrons is falling drastically with temperature as shown by photoconductivity measurements. The electrons are apparently falling into donor states.

Region 2 (15°K to 30°K). The remarkably constant current in this range presumably results from a balance between $e\phi_0/kT$ decreasing with increasing temperature and the mobility increasing.

Region 3 (above 30°K). The decrease in current is caused largely by an increase in α_L due to the attenuation of the sound by thermal phonons ²

This work was done in collaboration with J. R. A. Beale.

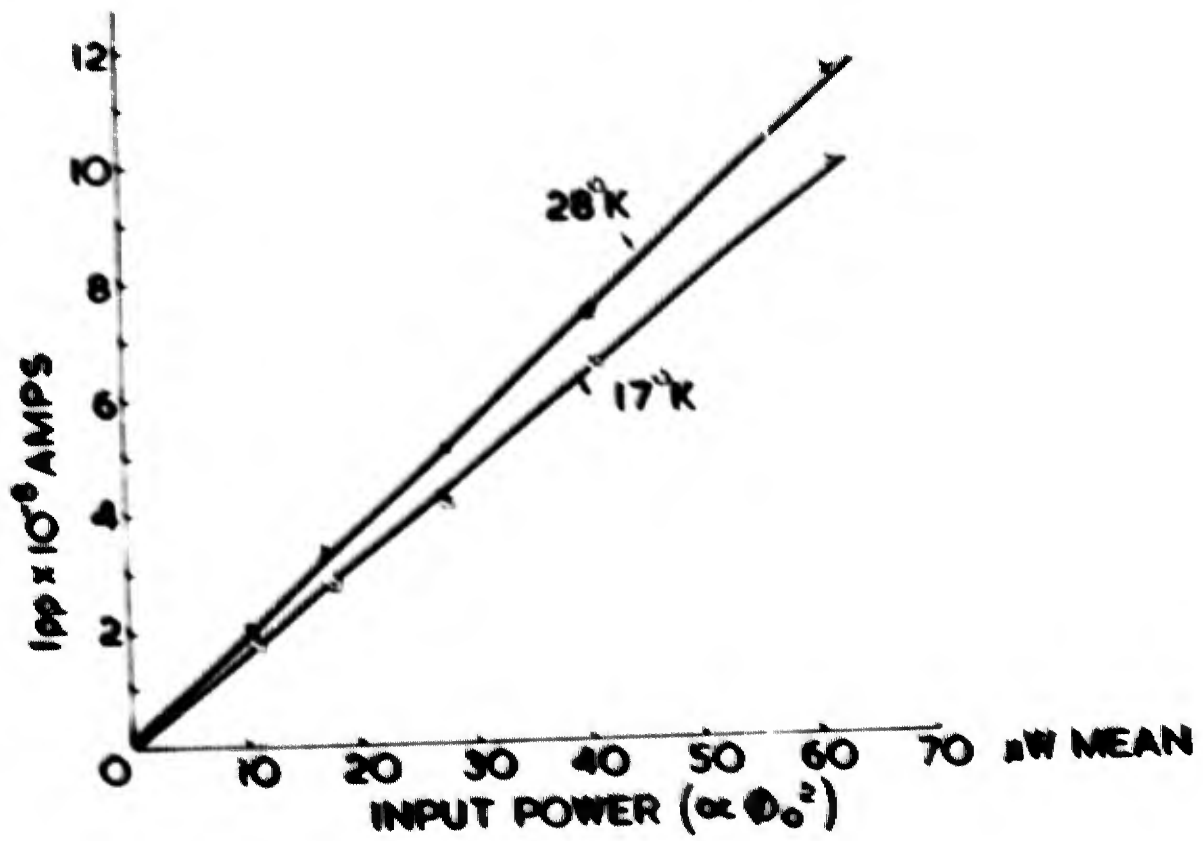


Figure 1 Peak to peak amplitude of acousto-electric current versus mean microwave power.

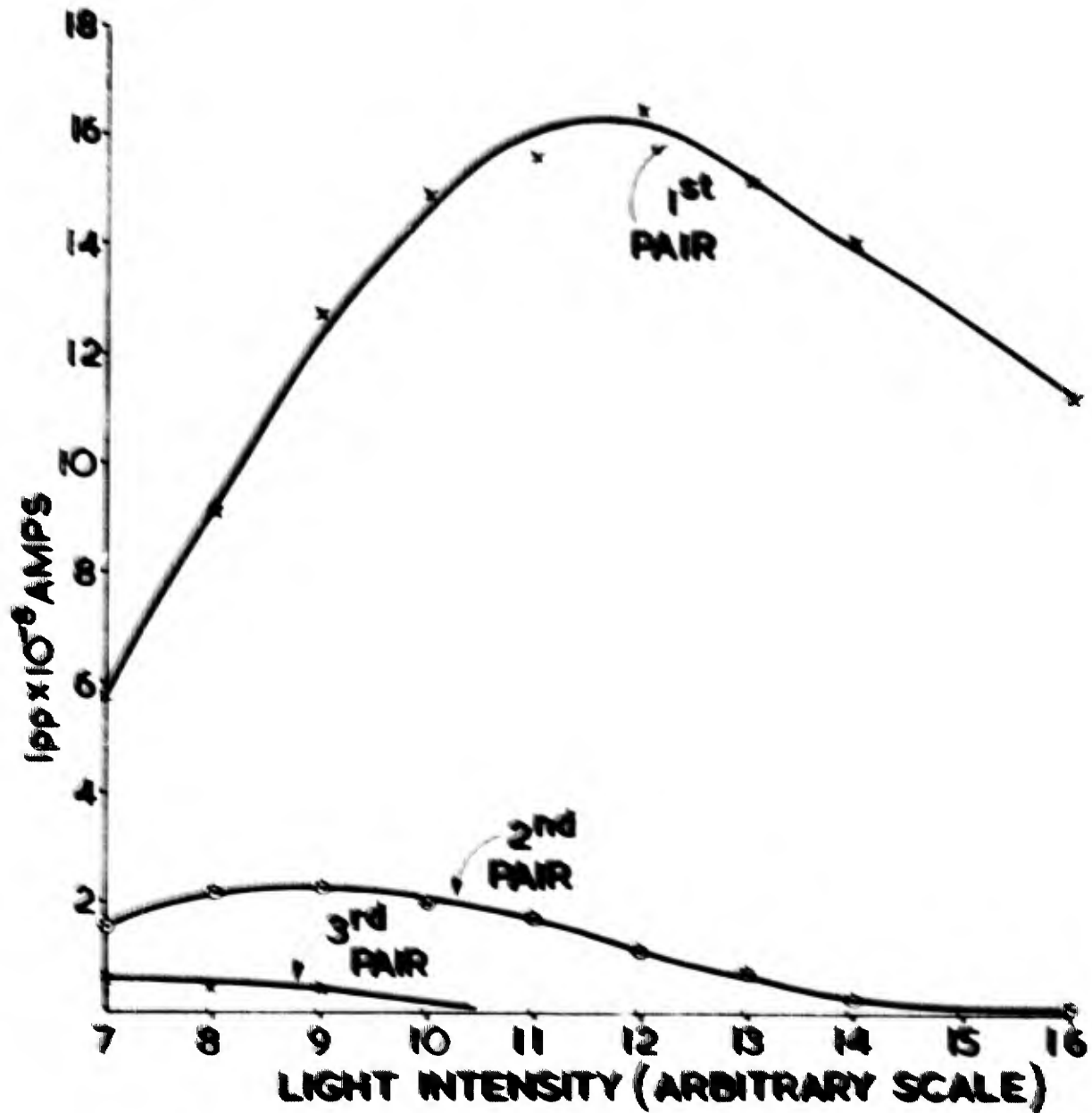


Figure 2 Peak to peak amplitude of acousto electric current at 25°K versus light intensity (arbitrary scale).

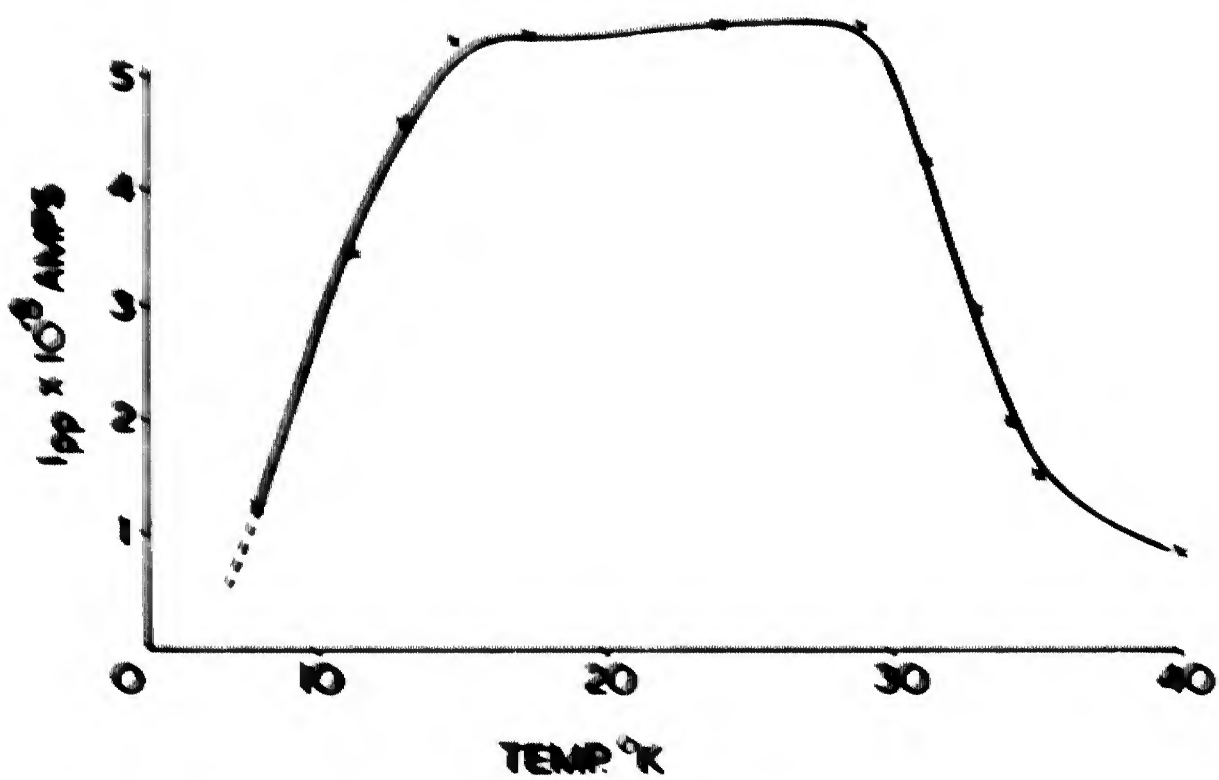


Figure 3 Temperature dependence of acousto-electric current.

B. Amplification of Microwave Phonons in Germanium

In order to achieve large amplification of phonons by electrons it is desirable to maximize the density of electrons carried by the wave. We consider the shear wave propagating in the (100) direction in Ge. This wave is one for which charge bunching is not accompanied by space-charge repulsion. This occurs because the shear increases the energy of two of the four equivalent (in zero strain) conduction-band minima while decreasing the energy of the other two by the same amount. This creates two classes of conduction minima for which the sum of the space charges in real space is a uniform density.

We calculated the attenuation of this shear wave, extending the theory of the acoustic-electric effect in n -Ge by including the effects of an applied electric field. The attenuation constant was found to be

$$\alpha = \frac{N e^2 \mu^2 \rho}{4 S^2 \rho} \frac{\omega^2 \tau_R (1 - v/S)}{1 + (1 - v/S)^2 \omega^2 \tau_R^2} \quad (2)$$

where N = electron density, μ = shear deformation - potential constant,

τ_R is a relaxation time ($\tau_R^{-1} = \tau_{IV}^{-1} + DQ^2$), τ_{IV} = intervalley relaxation time,

v = electron drift velocity, S = velocity of the acoustic wave,

ω = circular frequency of the acoustic wave, ρ = density of Ge.

Note that when $V > S$ the attenuation becomes negative, i.e., acoustic gain results when the electronic velocity exceeds the sonic velocity.

Values of Γ as a function of N and T are known for Ge from acoustic theory (see reference 1). We can use these values to estimate the

attenuation. Using (2), it is assumed that the electron parameters are the same as those of the phonons in the crystal. For $n = 10^{11}$ cm⁻³,

$N = 10^{16}$ cm⁻³, $\Gamma = 10^{-11}$ sec at 10^9 Hz and for $V = S$ the calculated gain is $\alpha = 0.20$ db/cm, a very large gain indeed for this device.

Experiments have been performed to determine the gain of the device. The samples were bars of single crystal Ge.

Dimensions of the (110) direction (width) of the (110) direction, with the z axis parallel to the z axis. The samples were 1 cm long and 0.5 cm²

in area. Pairs of 50 ohm dc contacts were applied to opposite corners of the ends of the samples. The phonons were generated in the longitudinal

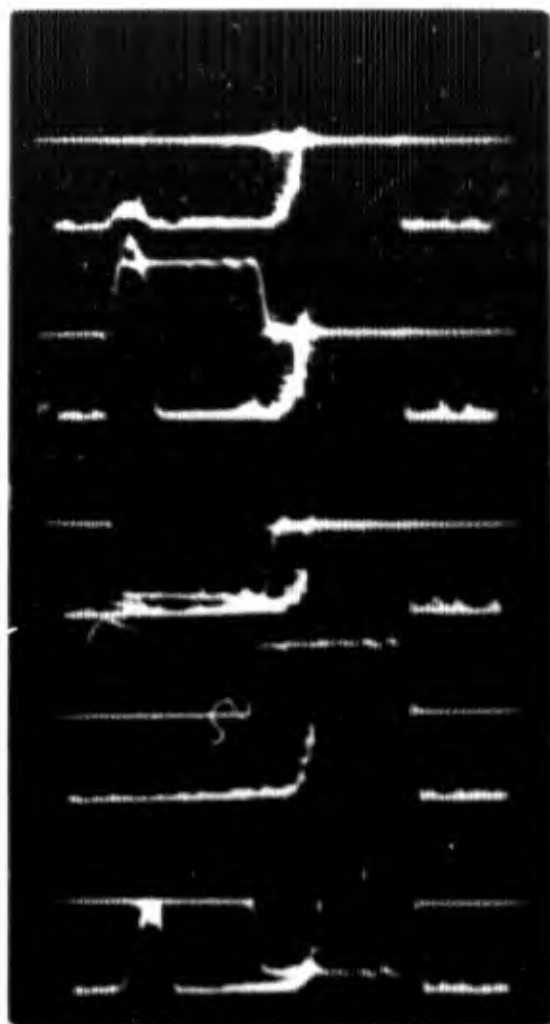
direction. The samples were cooled to liquid nitrogen. The gain was experimentally measured by using a sample containing 1×10^{11}

cm⁻³ electrons. The gain of the device at the resonance shows the gain is 0.20 db/cm. The gain of the device is such a small value that a large gain which


could be obtained if the phonons are truly generated. (The gain is the only quantity which can be measured and is picked up by the receiver.)

The actual gain of the device (direction) is the phonon value. The phonons are generated and detected at the same end of the crystal, hence



----- ELECTRONS
 ~~~~~~ PHONONS



a) NO CURRENT

b)   


c)   


d)   


e)   


PHONON PHONON  
 ECHO GENERATED

Figure 1. Phonon amplification in germanium. The times at which the phonons pulse is generated and its echo is received are indicated. The dashed arrows indicate the direction of the electronic current. The wavy arrows show the direction of propagation of the phonons during the time the current is applied. Details are given in the text.

they travel in two directions before a phonon echo is observed. A traveling wave interaction will be most effective if the electrons and phonons travel in the same direction, hence the electric pulse is applied either during the time the phonons are propagating away from the transducer or when they are returning to the transducer. The relative direction of the electrons can be changed by reversing the polarity of the pulse.

In exposure (a) of Fig. 1 is seen the phonon echo in the absence of electronic current. In (b) a pulsed current in which the electron drift velocity is about twice the phonon velocity is applied such that the electrons flow in the same direction as the phonons. An acoustic power gain of 20 db is observed. The electric field pulse acts to both liberate electrons by impact ionization of the donors and to impart a drift velocity to the electrons. In (c) the direction of the current is reversed, and the phonons are attenuated into the noise. In (d) the current pulse is advanced in time so that the current is now applied when the phonons are propagating away from the transducer. The positive current pulse now means that the electrons are flowing opposite to the phonon direction; attenuation is observed. In (e) the negative pulse now produces gain. The gain in (e) is less than that in (b) because the current produces some lingering lossiness (probably heating and thermal ionization which

attenuates the phonons during their return trip. These pictures show that the phonon power depends on the electron direction and velocity as expected for a traveling wave interaction.

Precise comparison of these experimental results with the theory, Eq. (1), is difficult because of experimental uncertainties about the area of the sample and the number of carriers present. The influence of impact ionization and the effect of the magnetic field (needed for the transducer) are not yet completely understood. It seems clear, however, that the observed amplification is less, by at least an order of magnitude, than the value predicted by Eq. (2). A suggested cause of this discrepancy is a breakdown of the assumption that the electronic properties are not affected by the applied electric field. It is known that the electrons can be "heated" by the electric field and that this heating changes the electronic transport properties. This possibility has been examined in more detail by Conwell, who estimated that the amplification may be reduced by a factor of order 50 by hot electron effects. The experimental results are in order of magnitude agreement with these estimates.

See Quarterly Progress Reports 1 and 5 for more details of this work.

### C. Heat Pulses in Metals

An investigation of heat pulses in single crystal metals and

semi-metals has also been made. The initial experiment on a polycrystalline tin sample showed that the electrons rather than the lattice were the principal heat carriers. The experimental arrangement was similar to that used for the heat pulse study in dielectric crystals.

The main purpose of this type of measurement was an attempt to measure the electron Fermi velocity directly. Single crystal tin, antimony, bismuth, aluminum and gallium crystals were investigated. Of these, only gallium was pure enough to have a noticeable temperature dependence in the shape of the detected pulse, i. e. a temperature dependent electron mean free path. In the other crystals the electrons are scattered frequently by impurities; we observed temperature independent diffusive heat arrival. We shall confine our discussion now to the work on Ga, which is more interesting.

The superconducting detector used in the experiments was different from the previous ones in that it was sensitive in the range 1.8-4.2°K. This made it possible to measure the temperature dependence without the use of a magnetic field to bias the superconductor.

The onset time, or the earliest time for which the heat pulse can be observed, was determined by those electrons



which travel with the least scattering. For the case where the electron mean free path is comparable to the sample dimension, the onset time represents that time required for ballistic electron flow at the Fermi velocity. However, the observed electron mean free paths were much shorter than the sample dimensions, resulting in diffusive heat flow. The maximum velocity that could be inferred from the data was  $v_F \geq 4 \times 10^7$  cm/sec. It is probable that there was still electron-phonon scattering (assuming impurity scattering can be neglected here) and that at lower temperatures the electron mean free path would be longer, which would reveal a yet greater Fermi velocity.

It was possible to obtain information about the electron mean free path,  $\Lambda$ , from the rate at which the heat pulse rises. For thermal diffusion, if a  $\delta$  function of heat is applied at a surface at  $x = 0$ , the temperature  $T$  at a surface at a distance  $x$  at time  $t$  is approximately

$$T \propto \frac{1}{\sqrt{t}} e^{-x^2/4Kt}$$

where  $K = \text{diffusivity} = \frac{1}{3} v_F \Lambda$ . Values of  $v_F \Lambda$  were derived from the data by measuring the time  $t$  in which  $T/T_{\text{max}} = 0.1$ . We found that  $\Lambda$  is proportional to  $T^{-3.0 \pm 0.3}$ . Theory predicts that the mean free path for electron-phonon collisions varies as

$T^{-3}$ .

Details of this work are given in the Quarterly Progress Reports 6 and 12.

#### D. Detection of Microwave Phonons Using Thin Film Bolometers

Microwave phonon echoes at 9.2 GHz have been observed using thin film detectors for both x-cut and AC quartz. The echoes were observed with In-Sn detectors similar to those used for the detection of heat pulses in the range 1.4-3.8°K. Transverse phonons in AC quartz were observed using pure indium films as detectors up to -12°K. Throughout this temperature range certain anomalies were observed in the echo pattern.

Because bolometers are detectors of energy it was expected that they would measure the rate of energy loss by the microwave phonons. The bolometer signals, however, were not observed to decrease exponentially; they had an irregular modulation on a generally decreasing pattern. The reasons for this behavior are not understood as yet. Another unexplained observation is the large magnitude of the attenuation of energy in the film. The observed attenuation is of the order of  $> 10^3$  db/cm. The theory of ultrasonic attenuation in a free-electron model (Pippard)

predicts order of magnitude lower attenuation. This discrepancy may arise from neglect by the theory of important properties of the real metal.

## CONCLUSIONS

Measurements of relaxation of  $\text{Ni}^{2+}$  paramagnetic ions were shown to be in agreement with theoretical calculations of avalanche relaxation in a phonon bottlenecked lattice. In the case of  $\text{Fe}^{2+}$  similar measurements could not be made, presumably due to a theoretically much faster avalanche time constant. However, phonons generated in  $\text{Fe}^{2+}$  avalanches were detected at one end of a 2.5 cm long crystal in which the spins were inverted on the opposite end. It was found that transverse phonon modes predominate in the avalanche. These "hot" phonon modes eventually decay by spin scattering to the cold modes.

Heat pulses have been observed in single crystal sapphire in the temperature range 4-54°K. Longitudinal and transverse modes are observable up to ~40°K with essentially no shift in the arrival time. Some scattering is present and the heat transport shifts from ballistic to diffusion flow in a continuous manner. Above 40°K, the transport is all by diffusion. The phonon mean free path calculated from the heat pulse data is in good agreement with the thermal conductivity mean free path. It appears that second sound is not as general a phenomenon as predicted and is not observed in sapphire.

We have observed ultrasonic echoes at 9.2 KMc using this

film bolometers in the normal and slightly superconducting states. The echo pattern is unexpectedly irregular and implies an anomalously large attenuation. In this present configuration these detectors do not appear useful for measuring the attenuation of  $\mu$ -wave phonon signals by the echo technique.



**FORMER STAFF/LEADS**  
**SECRET SERVICE/STAFF/LEADS**  
**STAFF/LEADS/STAFF/LEADS**  
**STAFF/LEADS**  
**STAFF/LEADS**

**STAFF/LEADS**

- 1. **ORGANIZATIONAL ACTIVITY** - From the name and address of the organization, determine the Department or the Bureau, activity, or other representative information which would be useful.
- 2. **STAFF/LEADS/STAFF/LEADS** - From the name of the organization, determine the name of the individual. "Members and Staff" is included. Making it to be in contact with appropriate security regulations.
- 3. **STAFF/LEADS** - Determine, if possible, in what Department, Bureau, or Office, or other representative information, the individual is currently employed. Also, when appropriate, determine the position held by the individual in the Department, Bureau, or Office.
- 4. **STAFF/LEADS** - From the complete name, title, or address, determine the name of the individual. If a nameplate, title, or other information is available, determine the name of the individual in all appropriate representative information, following the title.
- 5. **STAFF/LEADS** - If appropriate, determine the type of work, job, activity, program, committee, or other information which the individual holds when a specific reporting period is involved.
- 6. **STAFF/LEADS** - From the name, determine the name of the individual. From the name, determine the name of the individual. The name of the individual should be in contact with appropriate security regulations.
- 7. **STAFF/LEADS** - From the name of the individual, determine the name of the individual. From the name, determine the name of the individual. The name of the individual should be in contact with appropriate security regulations.
- 8. **STAFF/LEADS** - From the name of the individual, determine the name of the individual. From the name, determine the name of the individual. The name of the individual should be in contact with appropriate security regulations.
- 9. **STAFF/LEADS** - From the name of the individual, determine the name of the individual. From the name, determine the name of the individual. The name of the individual should be in contact with appropriate security regulations.
- 10. **STAFF/LEADS** - From the name of the individual, determine the name of the individual. From the name, determine the name of the individual. The name of the individual should be in contact with appropriate security regulations.

- 11. **STAFF/LEADS/STAFF/LEADS** - From the name and address of the organization, determine the Department or the Bureau, activity, or other representative information which would be useful.
- 12. **STAFF/LEADS/STAFF/LEADS** - From the name of the organization, determine the name of the individual. "Members and Staff" is included. Making it to be in contact with appropriate security regulations.
- 13. **STAFF/LEADS/STAFF/LEADS** - Determine, if possible, in what Department, Bureau, or Office, or other representative information, the individual is currently employed. Also, when appropriate, determine the position held by the individual in the Department, Bureau, or Office.
- 14. **STAFF/LEADS/STAFF/LEADS** - From the complete name, title, or address, determine the name of the individual. If a nameplate, title, or other information is available, determine the name of the individual in all appropriate representative information, following the title.
- 15. **STAFF/LEADS/STAFF/LEADS** - If appropriate, determine the type of work, job, activity, program, committee, or other information which the individual holds when a specific reporting period is involved.
- 16. **STAFF/LEADS/STAFF/LEADS** - From the name, determine the name of the individual. From the name, determine the name of the individual. The name of the individual should be in contact with appropriate security regulations.
- 17. **STAFF/LEADS/STAFF/LEADS** - From the name of the individual, determine the name of the individual. From the name, determine the name of the individual. The name of the individual should be in contact with appropriate security regulations.
- 18. **STAFF/LEADS/STAFF/LEADS** - From the name of the individual, determine the name of the individual. From the name, determine the name of the individual. The name of the individual should be in contact with appropriate security regulations.
- 19. **STAFF/LEADS/STAFF/LEADS** - From the name of the individual, determine the name of the individual. From the name, determine the name of the individual. The name of the individual should be in contact with appropriate security regulations.
- 20. **STAFF/LEADS/STAFF/LEADS** - From the name of the individual, determine the name of the individual. From the name, determine the name of the individual. The name of the individual should be in contact with appropriate security regulations.

~~CONFIDENTIAL~~

ALL INFORMATION CONTAINED HEREIN IS UNCLASSIFIED  
DATE 08-14-2001 BY 60322 UCBAW/STP

EXCEPT WHERE SHOWN OTHERWISE, THIS DOCUMENT IS UNCLASSIFIED  
DATE 08-14-2001 BY 60322 UCBAW/STP